THE FLORIDA STATE UNIVERSITY

COLLEGE OF ARTS AND SCIENCES

# THE RENDITION OF THE ATLANTIC WARM POOL IN REANALYSES

By

ASHLEY STROMAN

A Thesis submitted to the
The Department of Earth, Ocean and Atmospheric Science
in partial fulfillment of the
requirements for the degree of
Masters of Science

Degree Awarded:
Summer Semester, 2011

The members of the committee approve the thesis of Ashley Stroman defended on July 5, 2011.

_____
Vasubandhu Misra
Professor Directing Thesis

_____
Robert Hart
Committee Member

_____
Mark Bourassa
Committee Member

The Graduate School has verified and approved the above-named committee members.

I dedicate my thesis to my family. Without their support and encouragement, this work would not have been possible.

# ACKNOWLEDGEMENTS

I would like to acknowledge Dr. Vasu Misra who encouraged me to conduct this research and offered much guidance along the way. I would also like to thank Dr. Mark Bourassa and Dr. Robert Hart for answering questions related to my research and for serving on my committee. I would also like to thank Dr. Steven Chan who was very helpful in helping me learn programming languages, as well as for always being available for help. I'd like to thank the members of Dr. Misra's lab who were very helpful and encouraging during this process. I am forever grateful for my family. They have always been there for me and have always been supportive. Lastly, I'd like to thank my FSU friends. They have helped make my time here enjoyable inside and outside of school.

# TABLE OF CONTENTS

# LIST OF TABLES

# LIST OF FIGURES

# ABSTRACT

The Atlantic Warm Pool (AWP) is located in the western tropical North Atlantic (TNA) and the Intra-Americas Sea (IAS) (the Gulf of Mexico and the Caribbean Sea). The AWP is an area of warm sea surface temperatures (SSTs) greater than 28.5°C that exhibits a strong seasonal cycle, with the AWP disappearing in boreal winter (December-January-February) and reaching a maximum in late boreal summer (August-September-October (ASO)). In addition, the AWP exhibits interannual variability, with large AWPs nearly three times larger in area than small AWPs. Because there is a lack of surface and subsurface observations in the IAS and the TNA, this study uses reanalysis products to examine the AWP. It is of interest to ask what is the quality of these reanalysis products in their examination of the AWP. Thus, the main objective of this study is to examine and intercompare different reanalysis' renditions of the AWP.

Three ocean reanalysis products are examined in this study and they are the following: (1) the Global Ocean Data Assimilation System (GODAS), (2) the Climate Forecast System Reanalysis (CFSR), and (3) the Simple Ocean Data Assimilation (SODA). In addition, because GODAS and SODA are not coupled to the atmosphere whereas CFSR is, two atmospheric reanalysis products are also used and they are the following: (1) the NCEP–National Center for Atmospheric Research (NCAR) reanalysis (hereafter R1), and (2) the NCEP–Department of Energy (DOE) Atmospheric Model Intercomparison Project (AMIP-II) reanalysis (hereafter R2). R1 is used in conjunction with SODA, and R2 is used in conjunction with GODAS. The period of interest for this study is 1980–2006. Each ocean reanalysis is used to examine the annual and interannual variability of the AWP in ASO. In addition, GODAS with R2, CFSR, and SODA with R1 are used to perform a detailed analysis of the SST tendency equation of the AWP. Furthermore, GODAS with R2, CFSR, and SODA with R1 are used to examine the impact of the AWP on the tropical tropospheric temperature and see if the impact is similar to the impact seen by the El Niño Southern Oscillation (ENSO).

All three ocean reanalyses depict similar annual variability of the AWP. They all exhibit the AWP to be non-existent in boreal winter (December-January-February) and at a maximum in boreal summer. However, the reanalyses are inconsistent in their initial appearance of the AWP. All three ocean reanalyses depict similar interannual variability of the AWP; however, they are

inconsistent in the relationship between the AWP area and subsurface temperatures. From the SST tendency equation, the fluxes contribute more to the AWP SST tendency in GODAS and CFSR, and the fluxes act to remove heat from the AWP. In SODA, the advective terms contribute more to the AWP SST tendency. Additionally, the reanalyses show that the AWP warms the tropical troposphere contemporaneously (ASO) but not three to six months after, as in the case with ENSO.

# CHAPTER ONE

# INTRODUCTION

## 1.1 Objectives

Studies have examined the Atlantic Warm Pool (AWP) using in situ observations and general circulation models (Wang et al. 2006; Wang et al. 2007; Wang and Lee 2007; Wang et al. 2008). However, there is a lack of surface and subsurface observations in the Intra-Americas Sea (IAS) and western tropical North Atlantic (TNA), which is where the AWP is located (Figures 1.1 and 1.2). Compared to observations, reanalysis products have three benefits: (1) they are regular gridded datasets, (2) they exhibit high grid spacing, and (3) they provide data of variables that are not directly observed. However, there are four disadvantages to using reanalysis products: (1) the data exhibit inhomogeneities related to observing system changes, and the climate data output is sensitive to (2) resolution and physics of the numerical model, (3) the bias adjustment procedures for the assimilated data, and (4) the properties of the data assimilation system (Bengtsson et al. 2007). Therefore, it is of interest to examine the AWP using a reanalysis product and to study the quality of these reanalysis products in their rendition of the AWP. Thus, the main objective of this study is to examine and intercompare different reanalysis' renditions of the AWP.

## 1.2 Background and Motivation

### 1.2.1. The AWP

The AWP is characterized by an area of sea surface temperatures (SSTs) greater than or equal to 28.5°C as defined by Wang and Enfield (2001). It comprises the IAS (the Gulf of Mexico (Gulf) and the Caribbean Sea) and the western tropical North Atlantic. The AWP, which lies entirely north of the equator, has a seasonal cycle. The AWP disappears in boreal winter, December-January-February (DJF), and reaches its maximum areal extent in late boreal summer, August-September-October (ASO) as shown in Figure 1.3 (Wang et al. 2006; Wang et al. 2007; Wang and Lee 2007; Wang et al. 2008). Wang et al. (2006) showed the AWP exhibits

interannual variations where large warm pools are almost three times larger than small warm pools.

Wang et al. (2006) and Wang et al. (2008) showed that in boreal summer, anomalous AWPs have an impact on the climate in the Western Hemisphere, particularly the precipitation in northern South America, the Caribbean, and the Great Plains. In addition, they showed that anomalous AWPs have an impact on hurricane activity. There is a high population density in the IAS region, the United States, and northern South America, especially along the coastlines (Lewsey et al. 2004). Therefore, it is important to examine the AWP and its evolution as it has an impact on the climate and the human population in the IAS region, the United States, and northern South America.

## 1.2.2.Motivation

### 1.2.2.1. The AWP and Western Hemisphere Climate

In the summer, the North Atlantic subtropical high (NASH) has a well-defined core and is centered in the eastern subtropical North Atlantic. The NASH extends southwestward into the western North Atlantic, interacting with the northeastern portion of the AWP. In its southern portion, the NASH provides the tropical easterly trade winds, which transport warm water from the tropical North Atlantic into the Caribbean Sea (Wang et al. 2007; Wang et al. 2008; Wang and Lee 2007).

In the Caribbean Sea, the trade winds intensify due to the pressure gradient of the NASH and form the Caribbean Low Level Jet (CLLJ). Two times during the year (summer and winter) the CLLJ reaches a maximum, and two times during the year (fall and spring) it reaches a minimum. During the summer, the CLLJ is characterized as having a maximum of easterly zonal wind (~13 $ms^{-1}$) at roughly 925 mb (Wang et al. 2007; Wang and Lee 2007). As the CLLJ travels across the Caribbean Sea, it splits into two branches: one that travels northward and connects with the Great Plains low-level jet (GPLLJ), which moves across the Gulf and into the United States; and, one that continues traveling westward across Central America into the eastern North Pacific. The split occurs because there are two low pressure systems, one located in the eastern North Pacific (ENP) west of Central America and the other located over North America (Wang 2007; Wang and Lee 2007; Wang et al. 2007; Wang et al. 2008).

The AWP has been shown to weaken the NASH in the summertime, especially at its southwestern edge (Figure 1.4; Wang et al. 2008). This response was explained by Gill (1980), which says that for an off-equatorial heating anomaly, the atmospheric response is low sea level pressure to the northwest of the heating. Anomalous AWPs have an effect on the magnitude of the response. Large AWPs increase the atmospheric response, whereas small AWPs decrease the atmospheric response. Davis et al. (1993) showed that the NASH has implications on the weather and the climate in North America. The weakening of the NASH greatly impacts the movement of CLLJ and the GPLLJ, as well as the distribution of their associated moisture transport (Wang et al 2006; Wang et al. 2008).

Wang et al. (2006) and Wang et al. (2008) studied the effects of an anomalous AWP on the climate and precipitation in the Western Hemisphere. Wang et al. (2006) used observational data and focused on the ASO season. An AWP was categorized as large if it was 25% larger than the climatological mean area and small if it was 25% smaller. There were 14 large AWP events and 15 small AWP events. They found that the ASO rainfall variability in the northern Caribbean, southern Mexico, eastern South America, northwest United States, and Great Plains regions was mainly due to the size of the AWP. A large (small) AWP was positively (negatively) correlated with rainfall over the northern Caribbean and southern Mexico, whereas a large (small) AWP was negatively (positively) correlated with rainfall over the northwest United States, the Great Plains, and eastern South America. The relationship between the AWP and rainfall in the Caribbean is further justified from Hastenrath and Heller (1977). They found that the rainfall distribution in the tropical Americas is influenced by the interannual variability of SSTs in the tropical Atlantic. The relationship between the size of the AWP with rainfall in the Americas occurs because in the core region of a large (small) AWP, there is an anomalous increase (decrease) in convection, which is caused by the warm (cool) SST anomalies and a decrease (increase) in sea level pressure anomalies. Knaff (1997) showed that with a decrease (increase) in sea level pressure in the tropical Atlantic there is a decrease (increase) in subsidence, which increases (decreases) midlevel moisture. Therefore, these conditions contribute to a greater contemporaneous summer rainfall over the region surrounding the warm pool. There are two explanations for the relationship between the AWP and the Great Plains rainfall: (1) If there is more (less) moisture precipitating surrounding the large (small) AWP, then there is less (more) available moisture to be transported into the Great Plains, and (2) a large

(small) AWP weakens (strengthens) the GPLLJ, as well as disfavors (favors) moisture transport into the Great Plains, as shown in Figure 1.5 (Wang et al. 2006).

Wang et al. (2008) used the NCAR CAM3 atmospheric general circulation model to study the effects of anomalous AWP sizes on the summer (June-July-August) climate in the Western Hemisphere. For their study, they focused on the months July-August-September-October for the anomalous AWP size. If the warm pool was 33% larger than the climatological mean area, then it was considered a large AWP; if it was 33% smaller than the climatological mean area, then it was considered a small AWP. They identified six years as having large AWPs and seven years as having small AWPs. They showed that an anomalously large (small) AWP weakens (strengthens) the CLLJ and its moisture transport. Additionally, they showed that an anomalously large (small) AWP reduces (strengthens) the GPLLJ and its northward moisture transport. This change in moisture transport induced by the respective anomalous AWP contributes to the rainfall anomalies over southern Mexico, the Caribbean, and the Great Plains. In other words, a large (small) AWP increases (decreases) the summer rainfall over southern Mexico and the Caribbean, and decreases (increases) the summer rainfall over the Great Plains.

### 1.2.2.2. The AWP and Hurricane Activity

In the study from Vimont and Kossin (2007), it was shown that the Atlantic Meridional Mode (AMM), which is a meridional SST gradient near the inter-tropical convergence zone in the Atlantic Ocean, is at a maximum in boreal spring and is strongly correlated with hurricane activity in the boreal summer. The AWP is located in the region of the AMM, and thus, it also has an impact on hurricane activity (Wang et al. 2006; Wang et al. 2008). Wang et al. (2006) and Wang et al. (2008) showed that an anomalous AWP has an impact on hurricane activity. In these studies, they showed that an anomalously large (small) AWP leads to an increase (decrease) in hurricane activity. Both studies examined the relationship between the AWP and parameters such as SSTs warmer than 26º–27ºC (favorable temperatures for the development of deep convection), vertical wind shear, and convective available potential energy, which are three parameters important in the formation and development of a tropical storm (Gray 1979).

Wang et al. (2006) found that the ASO AWP area anomaly index combined with the SST anomalies in the tropical North Atlantic (domain: 6º–22ºN, 60º–15ºW) is positively and significantly correlated (at the 95% significance level) with hurricane activity in ASO. They

attributed this relationship to SSTs, which play a part in determining the maximum potential development of the storms. In addition, the temperatures required for development (temperatures greater than 26.0ºC) extend to a greater depth within the warm pool than elsewhere, thereby reducing the likelihood of cooler subsurface water to get mixed into the upper warm layer (Bender and Ginis 2000; Shay et al. 2000). Therefore, they concluded that the area over which the intensity and heat content are required for sustained development of storms is affected by the size of the warm pool, which makes the size of the warm pool very important in relation to hurricane activity. They also showed that the ASO AWP area anomaly index is negatively and significantly correlated (at the 95% significance level) with vertical wind shear. They explained the link between the AWP and hurricane activity using studies from Wang and Enfield (2001, 2003) and Knaff (1997). Wang and Enfield (2001, 2003) showed that the SST anomalies in the IAS are correlated with the sea level pressure anomalies in the IAS. Warm temperatures lead to a decrease in sea level pressure, which causes an anomalous increase in convective activity and cloudiness (Knaff 1997). In addition, there is also weak vertical wind shear, which helps organize deep convection, thereby strengthening the tropical storm and increasing hurricane activity in the Atlantic. In addition, Wang et al. (2006) showed that from 1950 to 2003, there were a larger number of major hurricanes (40) in years with large AWPs (14) than in years with small AWPS (24 major hurricanes in 15 years). Furthermore, they showed that two out of the eighteen years with small AWPs were during an active hurricane season whereas eight years were during an inactive hurricane season; for years with large AWPs, eleven of the eighteen years were during an active hurricane seasons and four years were during an inactive hurricane season. Therefore, Wang et al. (2006) concluded that large (small) AWPs favor (disfavor) hurricanes in the Atlantic.

Wang et al. (2008a) found that an anomalously large (small) AWP leads to a decrease (increase) in the vertical wind shear in the main development region (MDR). This reduction in vertical wind shear is explained by Gill (1980), which showed that the atmospheric response to the AWP's heating is baroclinic. To the northwest of the AWP, there is a cyclonic circulation in the lower troposphere, whereas there is an anticyclonic circulation in the upper troposphere. These tropospheric circulation patterns caused by the AWP reduce the easterly winds in the lower troposphere and the westerly winds in the upper troposphere, leading to a decrease in vertical wind shear. In the domain 10º–20ºN and 70º–30ºW, the average reduction in vertical

wind shear was roughly -0.9 $ms^{-1}$. In addition, they found that an anomalous AWP has an effect on convective available potential energy (CAPE). They found that an anomalously large (small) AWP increases (decreases) CAPE because of the increased (decreased) temperatures near the surface and the water vapor content. The difference in CAPE between large AWPs and small AWPs (large-small) ranged from 20 to 140 J $kg^{-1}$ in the tropical North Atlantic and from 20 to 40 J $kg^{-1}$ in the Gulf and the Caribbean Sea. An increase (decrease) in CAPE and a decrease (increase) in vertical wind shear are both favorable (unfavorable) conditions for hurricane development. Thus, an anomalously large (small) AWP leads to increased (decreased) hurricane activity because of a decrease (increase) in vertical wind shear in the MDR and an increase (decrease) in CAPE.

As just summarized, it is important to examine the AWP as it has an impact on the climate in the Western Hemisphere and on hurricane activity in the boreal summer. There is a lack of observations in the IAS and the western TNA, and it is worth asking what the quality of reanalysis products is in their rendition of the AWP. Therefore, this study examines and intercompares renditions of the AWP from reanalysis products. We will examine the annual and interannual variability of the AWP, as well as perform a SST budget analysis to examine whether advective terms or flux terms are the main contributing factors to the AWP SST tendency. In addition, we will study examine the impact of the AWP on the tropical tropospheric temperature and see if the impact is similar to the impact seen by the El Niño Southern Oscillation (ENSO). The data and methodology are described in Chapter 2, and the results of this study are detailed in Chapter 3. Conclusions are provided in Chapter 4, as well as ideas for future work.

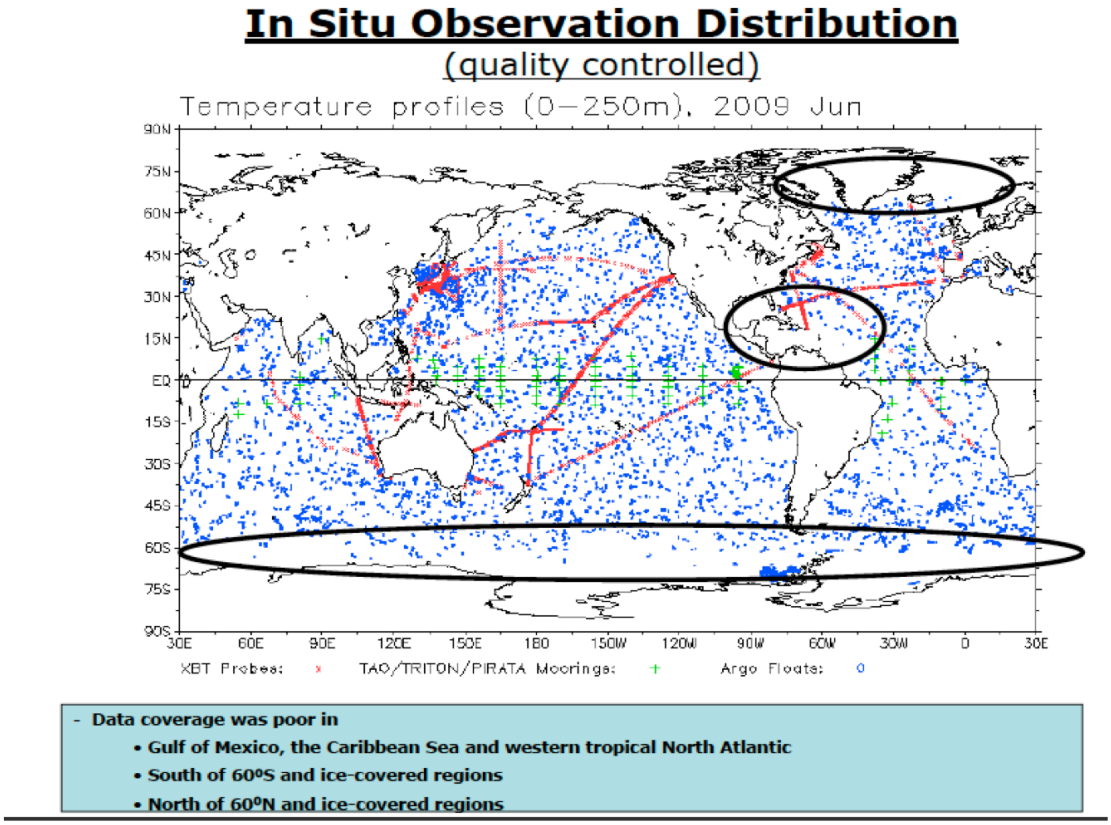


Figure 1.1. Temperature profiles (0-250m) in June 2009. Courtesy of Chunzai Wang, Atlantic Oceanographic and Meteorological Laboratory (AOML).

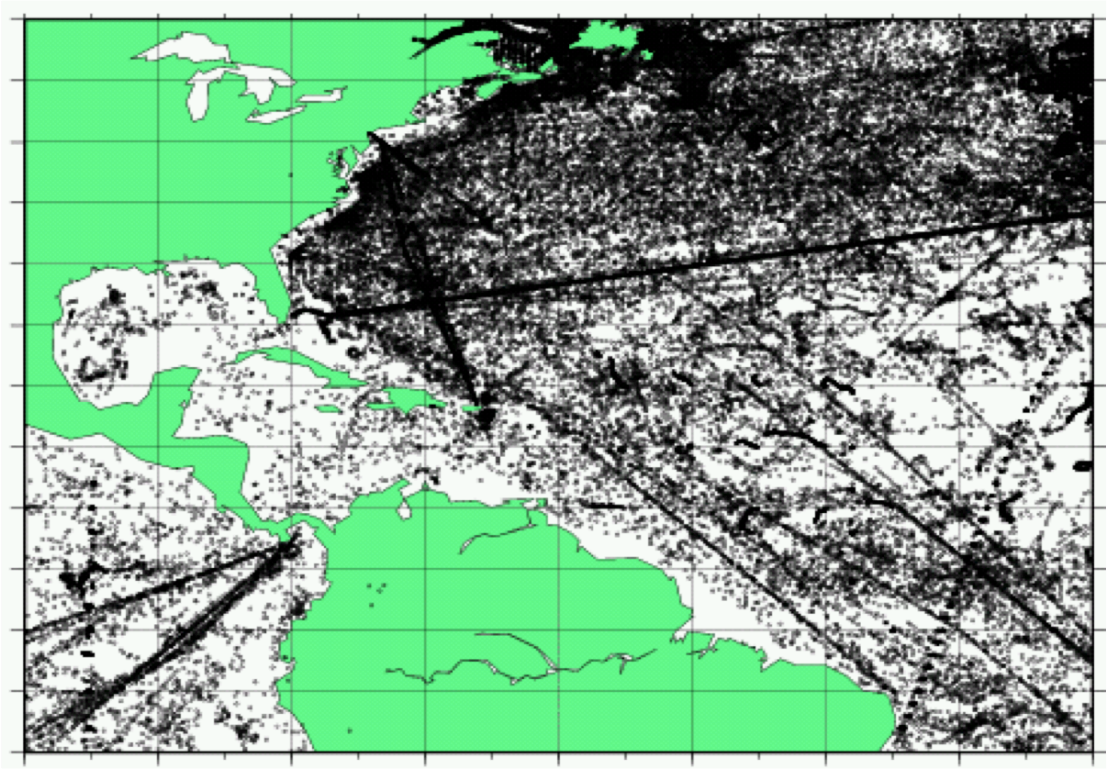

Figure 1.2. Location of observations that provided temperature profiles in the tropical North Atlantic, Caribbean Sea, and Gulf of Mexico during the period 1999-2005. Data were taken from the Global Transitioning System. Courtesy of Chunzai Wang, AOML.

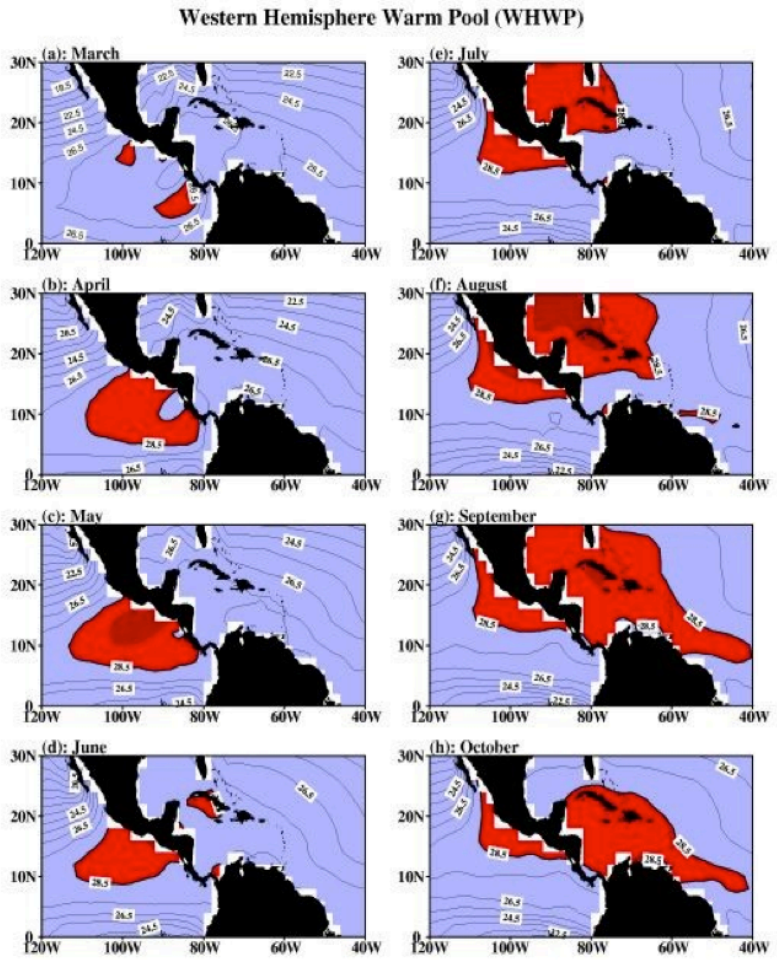


Figure 1.3. From Wang and Enfield (2003). Seasonal distribution of SSTs for the tropical Western Hemisphere warm pool: (a) March, (b) April, (c) May, (d) June, (e) July, (f) August, (g) September, and (h) October. The red shading represent water warmer than 28.5°C.

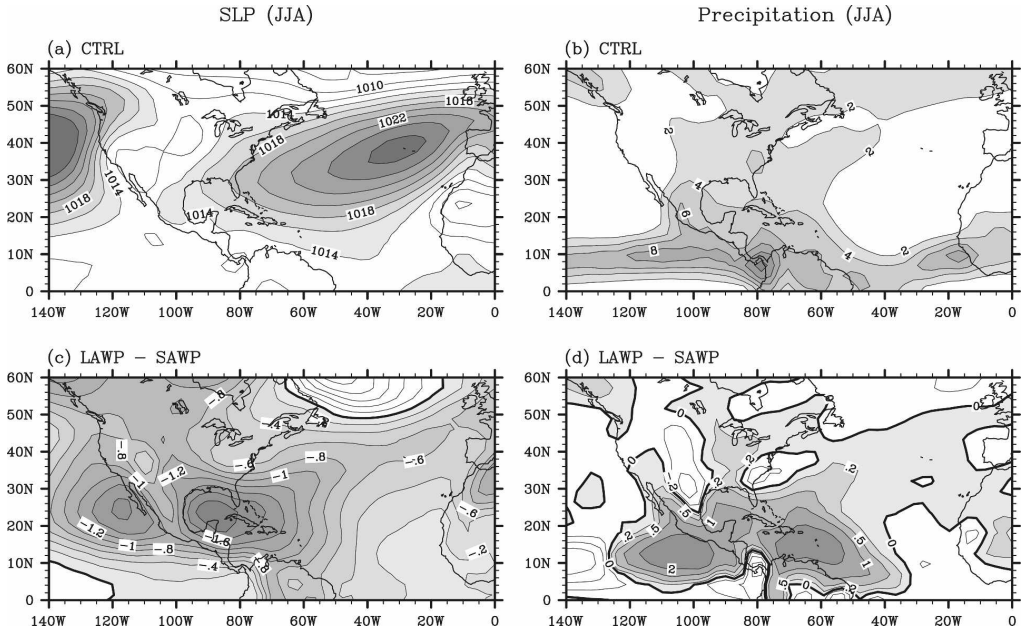


Figure 1.4. From Wang et al. (2008). (a) Sea level pressure (SLP) from the control run, (b) Precipitation from the control run, (c) SLP difference between the large AWP and small AWP runs, and (d) Precipitation difference between the large AWP and small AWP run. SLP units are mb and precipitations units are mm $day^{-1}$.

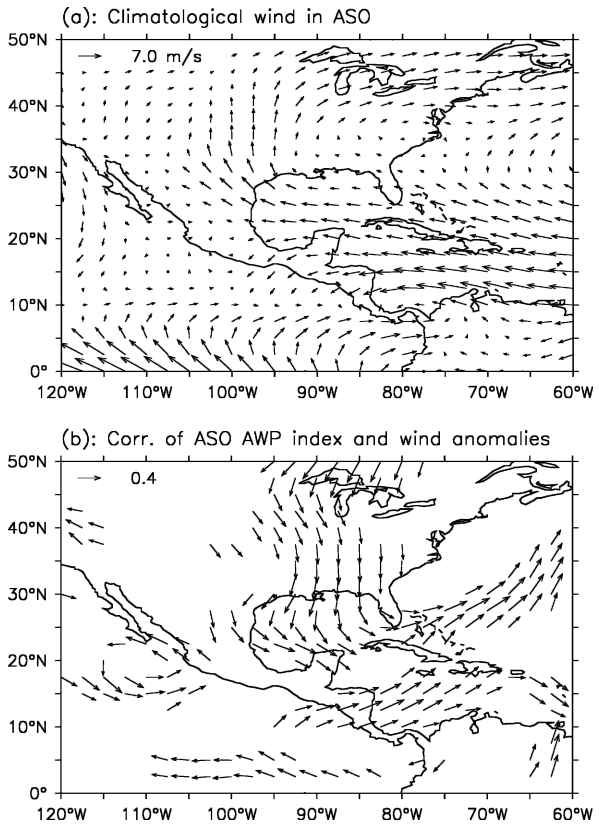


Figure 1.5. From Wang et al. (2006). Climatological wind at 925 mb during ASO, and (b) correlation of the ASO AWP index with the ASO 925 mb wind anomalies (only winds above the 95% significance level are plotted).

# CHAPTER TWO

# DATA AND METHODOLOGY

## 2.1 Reanalyses

The following five reanalysis products are used in the study: (1) the National Center for Environmental Prediction (NCEP) Global Ocean Data Assimilation System (GODAS; Behringer and Xue 2004) (2) the Simple Ocean Data Assimilation, version 2.1.6 (hereafter SODA; Carton and Giese 2008), (3) the NCEP–National Center for Atmospheric Research (NCAR) reanalysis (hereafter R1; Kalnay et al. 2006), (4) the NCEP–Department of Energy (DOE) Atmospheric Model Intercomparison Project (AMIP-II) reanalysis (hereafter R2; Kanamitsu et al. 2002), and (5) the NCEP Climate Forecast System Reanalysis (CFSR; Saha et al. 2010).

The GODAS and SODA are ocean reanalysis products and R1 and R2 are atmospheric reanalysis products; CFSR is a coupled atmosphere–ocean reanalysis product. Atmospheric variables from R1 and R2 are used in conjunction with the SODA and the GODAS reanalysis products, respectively. Atmospheric variables from CFSR are not used for GODAS and SODA because the ocean models in GODAS and SODA are forced with atmospheric variables from R2 and R1, respectively, and we wanted to remain consistent in this study. The reanalysis products, GODAS with R2, CFSR, and SODA with R1, are examined to see how each differs in its rendition of the AWP (Table 2.1). From these reanalysis products, we use monthly means from January 1980 to April 2007. The parameters used from each reanalysis product are listed in Table 2.2.

### 2.1.1. GODAS

This study incorporates ocean and land surface data from the GODAS, and the data are available from 1979 to the present. The ocean model is the Geophysical Fluid Dynamics Laboratory (GFDL) Modular Ocean Model version 3 (MOMv3) (Pacanowski and Griffies 1998).

The GODAS has a three-dimensional variational (3DVAR) data assimilation scheme that was devised by Derber and Rosati (1989). The quasi-global domain extends from 75°S to 65°N. The ocean model has a 1° longitudinal grid spacing and 1° latitudinal grid spacing, which is then enhanced to 1° longitudinal grid spacing and 1/3° latitudinal grid spacing within 10° of the equator. Additionally, there are 40 vertical levels with a resolution of 10 m in the upper 200 m. The GODAS is forced by fluxes (heat, momentum, and freshwater) from R2, and it assimilates temperature profiles (Behringer and Xue 2004). At the top model level, the SST is relaxed to weekly analyses of NCEP's blended analysis of in situ and satellite data (Reynolds et al. 2002).

### 2.1.2 SODA

Ocean data from the SODA are incorporated into this study. The ocean model in the SODA is based on the Los Alamos implementation of the Parallel Ocean Program version 2.1 (POP2.1; Smith et al. 1992). The model is constrained by temperature observations using a sequential assimilation algorithm, which is described by Carton et al. (2000a,b) and Carton and Giese (2008). The ocean model has 40 levels in the vertical, with 10 m resolution at the surface, and it has a grid spacing of 0.4° (longitude) x 0.25° (latitude). In addition, the Arctic Ocean is fully resolved since the pole is displaced (Carton et al. 2000a,b; Carton and Giese 2008; Zheng and Giese 2009).

The ocean model is forced with ERA-40 wind stresses for the period 1958–2001; for the period 2002–2008 it is forced by ERA-interim winds. Bulk formulae are used to calculate surface heat fluxes (Smith et al. 1992) and the atmospheric variables are taken from R1 (Kalnay et al. 1996). The model output, temperature and velocity, are mapped onto a uniform 0.5° x 0.5° grid, with 40 vertical levels (Zheng and Giese 2009).

### 2.1.3 R1

Upper-air and land surface data from R1 are included in this study. The data are available on a 2.5° x 2.5° grid (144 x 73) from 1948 to the present. The NCEP global spectral model (Kalnay et al. 1996) is the atmosphere model in R1. The model has a horizontal grid spacing of T62 (roughly 210 km) and 28 vertical sigma levels. The analysis scheme used is the spectral statistical interpolation (SSI), a three-dimensional variable (3DVAR) scheme that is cast in spectral space (Parrish and Derber 1992; Derber at al. 1991).

### 2.1.4 R2

This study incorporates upper-air data from R2, which are available on a 2.5° x 2.5° grid (144 x 73) from 1979 to the present. The atmosphere model in R2 is the NCEP global spectral model. R2 is considered to be an updated version of R1 because human processing errors were eliminated, parameterizations of physical processes were updated, and upgrades and improvements were made to the forecast model and diagnostic package (Kanamitsu et al. 2002).

### 2.1.5 CFSR

Upper-air, land surface, and ocean data from CFSR are included in this study. The reanalysis was produced by NCEP as a coupled atmosphere-ocean-land-sea ice system. The data are available from 1979 to the present. CFSR is considered to be superior to R1 and R2 because it involves a coupled system and has a higher global atmosphere resolution (horizontally and vertically) than R1 and R2. In addition, CFSR is a better reanalysis product than R1 and R2 for the following reasons: (1) It uses newer models and a more modern data assimilation system, (2) it is coupled to the ocean during the generation of the six-hour guess field, and (3) it directly assimilates satellite observations in radiance form instead of as retrieved values for variables such as temperature and humidity. The ocean initial conditions are from a stand-alone GODAS run with the ocean model, MOM4p0d.

The atmospheric model of CFSR is the operational Global Forecast System (GFS), and its assimilation scheme of the atmosphere data is the operational version of the Gridpoint Statistical Interpolation (GSI) (Kleist et al. 2009). The atmosphere model has a global grid spacing of T382 (~38 km) in the horizontal, and it has 64 vertical sigma-pressure hybrid levels. The operational GFS is coupled to the Noah LSM, which has four soil levels, and it is coupled to a two-layer sea-ice model (Wu et al. 2005).

The oceanic component of CFSR is the GFDL Modular Ocean Model version 4p0d (MOM4p0d), which is a finite difference model that assumes the Boussinesq and hydrostatic approximations. Compared to the ocean model used by the GODAS, MOM4p0d is fully global and has an interactive sea-ice model. The zonal grid spacing of MOM4p0d is 1/2°. The meridional grid spacing is 1/4° from 10°S to 10°N and it gradually increases in the tropics to 30°S and 30°N, at which point it becomes 1/2° toward the poles. MOM4p0d has 40 vertical

levels, with 27 in the upper 400 m of the ocean; the maximum depth is 4.5 km. The vertical resolution is 10 m from the surface to a depth of 240 m. The data assimilation system is the GODAS. SSTs are nudged to the daily OI SST (Reynolds et al. 2007).

## 2.2 Derived Variables

For this study, two calculations are performed using variables from native fields: the tropical tropospheric temperature and the oceanic depth of the 26.0°C and the 28.5°C isotherms. The tropical tropospheric temperature is calculated as monthly mean air temperature from 800 to 250 mb. The depth of the 26.0°C isotherm is calculated as monthly means using linear interpolation to measure the temperature depth between the vertical levels of the ocean models.

## 2.2 Methodology

We use monthly means from January 1980 to April 2007. First, monthly means of SSTs are found using GODAS, CFSR, and SODA to show the seasonal cycle of the AWP. Then, lead–lag correlations are performed between the AWP area and (1) global SST anomalies (SSTAs), (2) subsurface temperature anomalies (STAs), and (3) tropical tropospheric temperature (TT) anomalies using GODAS, CFSR, and SODA. The AWP area is composed of the anomalies of the area enclosed by the 28.5°C isotherm in ASO (domain: 0−40°N, 110−20°W). The SSTAs and STAs are calculated in ASO, as well as at a three and six month (or one and two seasons) lead and lag. Correlations involve the product of two variables. To calculate the time-lagged quantities, the product of variable $x$ at time $t$ with variable $y$ at time $t$+lag is found. Similarly, to calculate the time-lead quantities, the product of variable $x$ at time $t$ with variable $y$ at time $t$-lag is found. The lead–lag correlations give us atmospheric and oceanic perspectives on the surface and subsurface evolution of the AWP. They will help us determine if SST variations and temperature variations throughout the ocean depth in other parts of the globe are contributing to the evolution of the AWP, which will help us better examine the interannual variability of the AWP. In addition to lead–lag correlations, the depth of the 26.0ºC isotherm is calculated for the five years having the largest AWP area, as well as for the five years having the smallest AWP

area. To choose the five years with the largest and smallest AWPs, the area of the AWP in ASO were ranked for all 27 years from highest to lowest, and then the five years with the largest and smallest AWPs were used. The years having the largest and smallest AWPs are chosen to examine the hurricane heat potential between large AWPS and small AWPS.

In addition to the analysis methods described above, an analysis of the SST anomaly equation is performed to determine the mechanism for ocean temperature variation in the AWP. An SST anomaly tendency equation is produced if the equation is calculated for the upper 50 m of the ocean. Following the methods of Misra et al. (2008), the regression of the AWP SST tendency on the advective and flux terms in the SST tendency equation is plotted. This will allow us to diagnose the importance of the advective and flux terms on the AWP. The time tendency of the anomalous temperature is given in Equation (2.1) (Kang et al. 2001).

$$\frac{\partial T'}{\partial t} = -u_m \frac{\partial T'}{\partial x} - u' \frac{\partial T}{\partial x} - v_m \frac{\partial T'}{\partial y} - v' \frac{\partial T}{\partial y} - w_m \frac{\partial T'}{\partial z} - w' \frac{\partial T}{\partial z} - Q' \,, \tag{2.1}$$

where T is total temperature; u, v, and w are the zonal, meridional, and vertical velocity of the ocean, respectively; and Q is the total downward heat flux at the surface. Primes indicate anomalies, and the subscript "m" refers to means. The term to the left of the equal sign in Equation 2.1 is the time tendency of the SST anomaly. The six terms on the right hand side of the equal sign are as follows: (1) anomalous temperature advection by the mean zonal current, (2) advection of mean temperature by the anomalous zonal current, (3) anomalous temperature advection by the mean meridional current, (4) advection of mean temperature by the anomalous meridional current, (5) anomalous temperature advection by the mean vertical current, and (6) advection of mean temperature by the anomalous vertical current. In Equation (2.1), T is total temperature, i.e. $T=T_m+T'$. Thus, when partial differential of T is multiplied with either the mean current or anomalous current, double prime terms are produced. Since double prime terms are also included, it is assumed that there will be perfect balance between the two sides of Equation (2.1) as nothing is neglected or ignored. Additionally, Equation (2.1) assumes that the mean state of the AWP is steady throughout the year, and it also does not differentiate the stochastic noise from the signal as noise is implicitly included in the equation. This differentiation would be important to understand the differences in the rendition of the AWP between the reanalyses.

Table 2.1. List of reanalysis products along with the type and purpose of each reanalysis product

| **Reanalysis** | **Type** | **Used for?** |
|---|---|---|
| GODAS | Ocean | Compare |
| CFSR | Coupled (atmosphere and ocean) | Compare |
| SODA | Ocean | Compare |
| R1 | Atmosphere | Provide |
| R2 | Atmosphere | Provide |

Table 2.2. List of parameters used from the reanalysis products.

| | |
|---|---|
| Potential Temperature | GODAS, CFSR, SODA |
| U and V components of the Current | GODAS, CFSR, SODA |
| Total downward heat flux at the surface | CFSR |
| Latent Heat Flux | R1/R2 |
| Sensible Heat Flux | R1/R2 |
| Upward and Downward Longwave Radiation | R1/R2 |
| Upward and Downward Shortwave Radiation | R1/R2 |

# CHAPTER THREE

# RESULTS

This chapter begins with an examination of the annual variability of the AWP (section 3.1) followed by a section that examines the interannual variability of the AWP (section 3.2). In this section we will study the effects of surface and subsurface temperatures on the interannual variability of the AWP. In addition, the mean depth of the 26.0°C isotherm in ASO is studied between years exhibiting large AWP areas and years exhibiting small AWP areas. The third section (3.3) explores the SST budget of the AWP. This will help us understand the relative contribution of advective and flux terms to the AWP SST tendency. In section 3.4 we examine the atmospheric response to the AWP.

## 3.1 Annual Variability of the AWP

The seasonal cycle in GODAS is shown in Figures 3.1 and 3.2. The AWP is nonexistent from December through April. In May, the AWP appears to the south of Cuba. From June to September, the AWP includes the Gulf and the northern Caribbean Sea north of 15ºN. In October, the AWP is no longer located in the Gulf but is in the Caribbean Sea off the coasts of Costa Rica and Panama. In November, the AWP is located in the Caribbean Sea south of Cuba and north of Haiti and the Dominican Republic.

In CFSR, the AWP is nonexistent from December through May (Figures 3.3 and 3.4). In June it appears in the Caribbean Sea south of Cuba, north of Panama, and east of Belize, and it appears in the Gulf off the coast of Mexico. From July through August, the AWP is in the Gulf and in the Caribbean Sea north of 15ºN. In September, the AWP extends into the western tropical North Atlantic. In October, the AWP is no longer in the Gulf, and in November it is only off the southern coast of Cuba.

Figures 3.5 and 3.6 show the seasonal cycle of the AWP in the SODA. The AWP is nonexistent from December through March, and in April it appears in the Caribbean Sea off the coast of Mexico. In May, the AWP is present in the Caribbean Sea off the coasts of Panama,

Costa Rica, and Belize, and south of Cuba. In June and July, the AWP expands into the Gulf, and in August and September it extends into the western tropical North Atlantic. In October, the AWP is no longer in the Gulf, and in November, it is only present in the Caribbean Sea off the coasts of Belize, Costa Rica, and Panama.

The seasonal cycle of the AWP for all three reanalyses is similar. The AWP is nonexistent in boreal winter (December-January-February (DJF)) and at a maximum in late boreal summer (August-September-October). However, there are three notable differences: (1) the initial appearance of the AWP is different for all three reanalyses. The AWP appears in April, May, and June for the SODA, the GODAS, and the CFSR, respectively, (2) the SST fields of the SODA are less smooth in comparison to the fields of the GODAS and the CFSR, and (3) the GODAS does not have the AWP extend into the western tropical North Atlantic, whereas the CFSR and SODA do. The noisiness seen in SODA may be due to the fact that SSTs in the ocean model for SODA are not nudged to OISST data, whereas this is the case for GODAS and CFSR. However, this should be further examined as this is speculation.

## 3.2. Interannual variability of the AWP

To examine the interannual variability of the AWP, we perform lead−lag correlations between the AWP area and sea surface temperature anomalies (SSTAs) (section 3.2.1) and subsurface temperatures anomalies (STAs) (section 3.2.2). In this analysis, the AWP area in ASO is correlated with the SSTAs and STAs contemporaneously, and with the SSTAs and STAs leading the AWP area by three to six months and lagging the AWP area by three to six months. This can also be seen as a one and two season lead and lag. A six-month lead corresponds to February-March-April (FMA) of the same year, and a three-month lead corresponds to May-June-July (MJJ) of the same year. A three-month lag of the SSTAs and STAs corresponds to NDJ of the same year, and a six-month lag corresponds to FMA of the following year. For the correlations between the AWP area and the STAs, the depth at which the correlations of the two parameters are no longer statistically significant is plotted. Only values greater than 95% significance are shown, as defined by the critical value table for Pearson's Correlation Coefficient, for the figures in this section. The seasonal means (FMA, MJJ, ASO, and NDJ) are

assumed independent of one another, i.e. FMA is independent of MJJ, MJJ is independent of ASO, etc…

### 3.2.1. The AWP area and SSTAs

The lead−lag correlations for GODAS are shown in Figures 3.7 and 3.10. At a six-month lead (FMA) (Figure 3.7a), positive correlations are present in the western tropical North Atlantic, the eastern subtropical North Atlantic, and the North Atlantic south of Greenland. Positive correlations are also seen in the southwestern Indian Ocean. At a three-month lead (MJJ) (Figure 3.7b), positive correlations are present in the eastern subtropical North Atlantic, the western tropical North Atlantic, and the North Atlantic south of Greenland. There also exist positive correlations in the equatorial Indian Ocean. Contemporaneously (ASO) (Figure 3.7c), the AWP area is positively correlated with the SSTAs in the Gulf, the Caribbean Sea, the tropical North Atlantic, the North Atlantic south of Greenland, and in the Arabian Sea and Bay of Bengal. Three months after (NDJ) (Figure 3.10b), there are positive correlations in the Caribbean Sea, the tropical North Atlantic, and the North Atlantic south of Greenland. At a six-month lag (FMA) (Figure 3.10c), there are positive correlations in the North Atlantic south of Greenland.

Figures 3.8 and 3.11 show the lead−lag correlations for CFSR. At a six-month lead (FMA) (Figure 3.8a), positive correlations are present in the western tropical North Atlantic and the eastern subtropical North Atlantic. Positive correlations are also seen in the southwestern Indian Ocean and in the North Atlantic south of Greenland. At a three-month lead (MJJ) (Figure 3.8b), positive correlations are present in the eastern subtropical North Atlantic, the western tropical North Atlantic, and in the North Atlantic south of Greenland. Contemporaneously (ASO) (Figure 3.8c), the AWP area is positively correlated with the SSTAs in the Gulf, the Caribbean Sea, the tropical North Atlantic, and the North Atlantic south of Greenland. In addition, there are positive correlations between the AWP area and SSTAs in the Arabian Sea and Bay of Bengal and in the North Atlantic south of Greenland. Furthermore, the AWP area is negatively correlated with the SSTAs in the Arctic. Three months after (NDJ) (Figures 3.11b), there are positive correlations in the Caribbean Sea and in the tropical North Atlantic. Additionally, there are positive correlations in the western Pacific and North Atlantic south of Greenland, and these positive correlations extend for the next three months (FMA).

The lead−lag correlations for SODA are shown in Figures 3.9 and 3.11. At a six-month lead (FMA) (Figure 3.9a), positive correlations are present in the western tropical North Atlantic, the eastern subtropical North Atlantic, and the North Atlantic south of Greenland. Positive correlations are also seen in the southwestern Indian Ocean. At a three month-lead (MJJ) (Figure 3.9b), positive correlations are present in the eastern subtropical North Atlantic, western tropical North Atlantic, and the North Atlantic south of Greenland. There exist positive correlations in the equatorial Indian Ocean and in the Arctic Ocean. Contemporaneously (ASO) (Figure 3.9c), the AWP area is positively correlated with the SSTAs in the Gulf, the Caribbean Sea, the tropical North Atlantic, and the North Atlantic south of Greenland. In addition, there are positive correlations between the AWP area and SSTAs in the Arabian Sea and Bay of Bengal and in the North Atlantic south of Greenland. Three months after (NDJ) (Figures 3.11b), there are positive correlations in the Caribbean Sea, the tropical North Atlantic, and in the North Atlantic south of Greenland.

The interannual variability of the AWP is similar in all reanalyses. All reanalyses show a relationship between the AWP area and SSTAs in the eastern subtropical North Atlantic, the western tropical North Atlantic, and the North Atlantic south of Greenland contemporaneously, as well as at a three and six-month lead (SSTAs leading). However, there are notable differences between the reanalyses: (1) the spatial extent of the correlations in the North Atlantic south of Greenland is larger in the CFSR, (2) the GODAS shows no significantly positive correlations in the Caribbean Sea and the tropical North Atlantic six months after (FMA) whereas the CFSR and SODA do, (3) at a three-month lead (MJJ), the AWP area is positively correlated with SSTAs in the Gulf in the CFSR and the SODA but not in the GODAS, (4) at a three-month lead (MJJ), the SODA is not showing positive correlations between the AWP area and the SSTAs in the Caribbean Sea south of Cuba whereas the GODAS and the CFSR are, and (5) the CFSR is showing positive correlations between the AWP area and the western Pacific contemporaneously as well as three months (NDJ) and six months after (FMA).

### 3.2.2. The AWP area and STAs

The lead−lag correlations for GODAS are shown in Figures 3.13 and 3.16. At a six-month lead (FMA) (Figure 3.13a), STAs roughly 200 m below the ocean surface in the western tropical North Atlantic and eastern subtropical North Atlantic are positively correlated with the

AWP area. Additionally, there is a positive correlation between the AWP area with STAs in the North Atlantic south of Greenland to a depth of 1000 m. At a three-month lead (MJJ), there are positive correlations nearly 200 m below the ocean surface in the western tropical North Atlantic and the eastern subtropical North Atlantic. STAs to a depth of 5 m in the Gulf are positively correlated with the AWP area. In the North Atlantic, the CFSR has STAs to a depth of 700 m positively correlated with the AWP area. Additionally, off the coast of Venezuela, the GODAS reanalysis shows positive correlations of STAs to a depth of 500 m. Contemporaneously (ASO) (Figure 3.13b), the GODAS shows positive correlations to a depth of 5 m in the Gulf and to a depth of 200 m in the tropical North Atlantic and the eastern subtropical North Atlantic. The GODAS show STAs positively correlated in the Caribbean Sea to a depth of 85 m and to a depth of 500 m along the coast of South America. Additionally, there are positive correlations between the AWP area and STAs to a depth of 150 m along the equatorial Atlantic. Furthermore, North Atlantic STAs to a depth of 500 m are positively correlated to the AWP area. At a three-month lag (NDJ) (Figure 3.16b), STAs below 5 m in the Gulf are not correlated with the AWP area. STAs 85 m below the ocean surface in the Caribbean Sea and the tropical North Atlantic are positively correlated to the AWP area. Additionally, STAs in the North Atlantic are positively correlated to depths of 1000 m south of Greenland and extending to Iceland. At a six-month lag (FMA) (Figure 3.16c), the GODAS shows positive correlations in the North Atlantic to a depth of 4000 m. Additionally, the AWP area is positively correlated with STAs in the North Atlantic from 200 m to 2500 m below the ocean surface south of Greenland to Iceland.

The lead−lag correlations for CFSR are shown in Figures 3.14 and 3.17. At a six-month lead (FMA) (Figure 3.14a), STAs roughly 200 m below the ocean surface in the western tropical North Atlantic and eastern subtropical North Atlantic are positively correlated with the AWP area. There are also positive correlations between the AWP area and STAs in the North Atlantic south of Greenland to depths of 4000 m. Additionally, in the Caribbean Sea, the CFSR shows positive correlations to a depth of 200 m. At a three-month lead (MJJ) (Figure 3.14b), there are positive correlations nearly 200 m below the ocean surface in the western tropical North Atlantic and the eastern subtropical North Atlantic. In the CFSR, STAs to a depth of 50 m in the Gulf are positively correlated with the AWP area. In the North Atlantic, the CFSR has STAs to a depth of 4000 m positively correlating with the AWP area. Additionally, off the coast of Venezuela, there are positive correlations between the AWP area and STAs to a depth of 400 m.

Contemporaneously (ASO) (Figure 3.14c), the CFSR shows positive correlations to a depth near 5 m in the Gulf and 200 m in the tropical North Atlantic and the eastern subtropical North Atlantic. The CFSR shows positive correlations between the AWP area and STAs to a depth of 200 m in the Caribbean Sea and to a depth of 150 m along the equatorial Atlantic. Furthermore, STAs in the North Atlantic are positively correlated to the AWP area extending to a depth of 4000 m below the surface and extending from south of Greenland all the way to Europe. At a three-month lag (NDJ) (Figure 3.17b), STAs below 5 m in the Gulf are not positively correlated with the AWP area. STAs 85 m below the ocean surface in the Caribbean Sea and the tropical North Atlantic are positively correlated to the AWP area and there are also positive correlations nearly 150 m in the eastern tropical North Atlantic. Additionally, there is a positive correlation between the AWP area and STAs in the North Atlantic to depths near 4000 m south of Greenland to Europe. At a six-month lag (FMA) (Figure 3.17c), there are positive correlations in the tropical North Atlantic and eastern subtropical North Atlantic to a depth of 150 m below the sea surface. Also, there are positive correlations with STAs in the Caribbean Sea south of Haiti and the Dominican Republic 50m to 100 m below the ocean surface. Additionally, the AWP area is positively correlated with STAs in the North Atlantic 200 m to 2500 m below the ocean surface south of Greenland to Ireland.

The lead−lag correlations for SODA are shown in Figures 3.15 and 3.18. At a six-month lead (FMA) (Figure 3.15a), STAs roughly 200 m below the ocean surface in the western tropical North Atlantic and eastern subtropical North Atlantic are positively correlated with the AWP area. Also, there are positive correlations between the AWP area and STAs in the North Atlantic south of Greenland to depths as low as 200 m. At a three-month lead (MJJ) (Figure 3.15b), there are positive correlations between the AWP area and STAs nearly 200 m below the ocean surface in the western tropical North Atlantic and the eastern subtropical North Atlantic. Also, there are positive correlations between the AWP area and STAs to a depth of 50 m in the Gulf. In the North Atlantic, the CFSR has STAs to a depth of 400 m positive correlating with the AWP area. Additionally, off the coast of Venezuela, there are positive correlations of STAs to a depth of 200 m. Contemporaneously (ASO) (Figure 3.15c), there are positive correlations between the AWP area with STAs in the Caribbean Sea to a depth of 85 m and to a depth of 150 m along the equatorial Atlantic. Furthermore, there are positive correlations between the AWP area and STAs in the North Atlantic extending to depths of 500 m. At a three-month lag (NDJ) (Figure 3.18b),

STAs below 5 m in the Gulf are not positively correlated with the AWP area, and STAs 85 m below the ocean surface in the Caribbean Sea and the tropical North Atlantic are positively correlated to the AWP area. Additionally, there is a positive correlation between the AWP and STAs in the North Atlantic to depths near 1000 m along the coast of Greenland. At a six-month lag (FMA) (Figure 3.18c), there are positive correlations in the tropical North Atlantic and eastern subtropical North Atlantic to a depth of 1000 m below the ocean surface, mainly south of Iceland.

The interannual variability of the AWP is similar in all reanalyses. All three reanalyses show positive correlations between the AWP area and STAs contemporaneously, and at a three and six-month lead (STAs leading), in the western tropical North Atlantic and eastern subtropical North Atlantic extending to a depth of 200 m. At a three-month lag (NDJ), all reanalyses show that STAs in the Gulf are not positively correlated with the AWP area. However, there are notable differences between the reanalyses: (1) the SODA does not show any significant correlation between the AWP area with STAs below 200 m in the Caribbean Sea and tropical North Atlantic in any lead−lag relationship, (2) the CFSR shows significant correlations between the AWP area (ASO) and STAs in the North Atlantic extend to lower depths than in the GODAS and the SODA, (3) the GODAS shows no significant correlations below 5 m in the Gulf, Caribbean Sea, and tropical North Atlantic at a six-month lag (FMA), (4) at a three-month lead (MJJ) and contemporaneously (ASO), there are positive correlations between the AWP area and STAs off the coast of South America to depths of 500 m in the GODAs, which is at lower depths than in SODA and CFSR, and (5) the results in SODA are “noisy” compared to GODAS and CFSR.

The relationship between the AWP and subsurface temperatures south of Greenland in CFSR could be deep-water formation. Furthermore, the relationship between the AWP and subsurface temperatures in the tropical Atlantic in ASO in all three reanalyses could be from Mediterranean Water. In addition, the relationship between the AWP and subsurface ocean temperatures in AS for all three reanalyses could be from outflow from the Amazon and Orinoco Rivers. One reason for the discrepancies between the reanalyses is that GODAS and CFSR use the MOM ocean model whereas SODA uses the POP. In addition, a reason for CFSR showing statistically significant correlations to lower depths compared to GODAS is that the CFSR uses a newer version of MOM. However, this is purely speculation and should be further examined.

### 3.2.3. The depth of the 26.0°C isotherm

In section 1.2.2.2, it was discussed how large (small) AWPs favor (disfavor) hurricane intensification and formation. One necessary, but insufficient, condition for hurricane formation are temperatures greater than 26.0°C (Holland 1997). Leipper and Volgenau (1972) showed that the depth of the 26.0°C isotherm is proportional to hurricane heat potential. Thus, in this section we calculate the depth of the 26.0°C isotherm to examine hurricane heat potential for large AWPs and small AWPs. In all reanalyses, the mean depth of the 26.0°C isotherm is examined for the five years with the largest AWP area and the five years with the smallest AWP area. In this analysis, the AWP area is composed of the mean area enclosed by the 28.5°C isotherm in ASO. Table 3.1 shows the five years with the largest AWP, and Table 3.2 shows the five years with the smallest AWP; the AWP area is also given for each year.

In all three reanalyses, the mean maximum depth of the 26.0°C isotherm is larger for small AWPS than large AWPs by roughly seven to ten meters (Figures 3.19, 3.21, and 3.23). The standard deviation of the mean depth of the 26.0°C isotherm is shown in Figures 3.20, 3.22, and 3.24. Additionally, in small AWPs, the 26.0°C isotherm extends to lower depths in the Gulf, the Caribbean Sea, and the tropical Atlantic compared to large AWPs. Based on the findings from Leipper and Volgenau (1972), small AWPs have a higher hurricane heat potential compared to large AWPs. However, if we volume integrate the hurricane heat potential for large and small AWPs, large AWPs have a higher hurricane heat potential than small AWPs. This should be further examined in future work. Furthermore, the mean maximum depth in GODAS in large and small AWPs is more similar to the mean maximum depth in SODA than CFSR. This may be due to the fact that GODAS and SODA are not coupled reanalyses, however, there is speculation and should be further examined.

## 3.3 SST Anomaly Equation

Calculating the covariance of the time derivative of the AWP SST anomaly with each term of the SST anomaly equation helps us determine the mechanism (advection or fluxes) of the ocean temperature variation of the AWP throughout the year. The aim is not to estimate the budget of the AWP SST, but instead to evaluate the relative importance and contribution of the

advective and flux terms in the SST equation. It is important to note that though advective processes and fluxes on shorter time scales than a month may be important in the monthly AWP SST anomalies, consideration of sub-monthly variations is beyond the scope of this work.

The results in Figure 3.25 and 3.26 suggest that the dominant term is the anomalous flux term in the GODAS with R2, and the anomalous flux term negatively contributes to the AWP SST tendency. From the advective terms, the anomalous vertical advection shows little correlation, whereas the mean vertical advection shows positive correlations along the equator in the eastern Pacific. The mean zonal advection in the far eastern Pacific and the anomalous meridional advection along the northern coast of South America have a positive relationship with the AWO SST tendency, whereas the anomalous meridional advection shows a negative relationship with the SST tendency north of the equator in the eastern Pacific. The zonal and meridional advective terms are positively and negatively correlated along the northern coast of South America.

Figures 3.27 and 3.28 shows that the dominant term is the anomalous flux term in the CFSR. The anomalous flux term shows a relationship similar to that seen in the GODAS with R2; the anomalous flux term negatively contributes to the AWP SST tendency. The mean vertical advection shows a pattern similar to that seen in GODAS with R2 but with lower magnitude. Furthermore, in the far eastern Pacific and north of the equator in the eastern Pacific, the correlation of the mean vertical advection is the opposite sign from what is shown in the GODAS. Additionally, the mean meridional advection in the equatorial Eastern Pacific is the opposite sign from what is seen in the GODAS with R2. The zonal and merdional advective terms have greater positive and negative correlations along the coast of South America, in the Gulf, and around the Florida peninsula than in the CS and the TNA.

The advective terms (except the anomalous vertical advection term) are (positively and negatively) contributing more than the anomalous flux term in the SODA with R1 reanalysis (Figure 3.29 and 3.30). The mean zonal advection shows positive and negative correlations off the northern coast of South America, the Caribbean Sea and the Gulf. The mean meridional advection shows positive correlations north of the equator in the eastern Pacific and off the northern coast of South America, as well as in the Caribbean Sea and the Gulf. The mean vertical advection shows positive correlations in the eastern Pacific, as well as negative and positive correlations collocated with the Loop Current and Gulf Stream.

All three reanalyses show the advective terms in the eastern Pacific positively and negatively contributing to the AWP SST tendency. In addition, in all three reanalyses, advective terms positively and negatively contribute to the AWP SST tendency along the northern coast of South America, the Caribbean Sea, and in the Gulf collocated with the Loop Current, as well as in the Atlantic collocated with the Gulf Stream. In the GODAS with R2 and the CFSR, the flux terms contribute more to the AWP SST tendency, whereas the advective terms in the SODA with R1 are the main contributor to the AWP SST tendency. Thus, in all three reanalyses, advection expands and contracts the area of the AWP throughout the year, and the surface heat fluxes contract the area of the AWP throughout the year.

The figures for SODA are noisy compared to the figures for GODAS and CFSR. This could be due to the ocean model that SODA uses (POP) along with the data from R1, which, as mentioned in section 2.1.4, was known to possess human errors. Additionally, in the ocean models used by GODAS and CFSR (MOM), the resolution in the top 200 m is 10 m, which could also explain the discrepancies found between the reanalyses. However, this should be further examined as this is purely speculation.

## 3.4 Atmospheric Response to the AWP

In this study, we first examine the relationship between ENSO and TT anomalies in GODAS with R2, CFSR, and SODA with R1 to see if the reanalyses are showing a similar result as Chang and Sobel (2002), which is that the global tropical troposphere warms three to six months after an ENSO event. In addition, we examine the relationship between the area of the AWP and TT anomalies. Our objective is to see if the AWP has a similar impact on the global tropical troposphere similar to the impact seen from an ENSO event.

For this study, TT anomalies are defined as the monthly 850-200 mb tropospheric temperature anomalies. The Niño-3 index (defined as the SST anomaly averaged over 5°N-5°S and 150°-90°W) is used to describe ENSO, and it is calculated for September-October-November (SON). This is correlated with the TT anomalies contemporaneously, as well as with the TT anomalies in DJF and March-April-May (MAM); TT anomalies in DJF and MAM are lagging the Niño -3 index. In addition, the AWP area is composed of the anomalies of the area enclosed by the 28.5°C isotherm in ASO. In this analysis, the AWP area in ASO is correlated

with the TT anomalies contemporaneously, as well as lagging the AWP area by three months (NDJ) and six months (FMA).

Spatially the correlations between the Niño -3 index and the TT anomalies are the same in all three lead–lag relationships for all three reanalyses. In all three, the entire tropical troposphere is warmed three months after (DJF) (Figures 3.31b, 3.32b, and 3.33b) and six months after (MAM) (Figures 3.31c, 3.32c, and 3.33c) the ENSO event. Furthermore, three months after the ENSO event (DJF), there are correlation values greater than 0.9 in the eastern Pacific Ocean for all three reanalyses. However, there are noticeable differences between the reanalyses. First, in the contemporaneous correlation (Figures 3.31a, 3.32a, 3.33a), the "dumbbell" shape given by the positive correlations is more noticeable in the GODAS and the SODA. In the CFSR, positive correlations straddle the equator, and in the western and central equatorial Pacific there are negative correlations, which are not seen in the GODAS and the SODA reanalyses. Lastly, three months after the ENSO (DJF), event the positive correlations do not extend to the far western Pacific in the CFSR as they do in the GODAS and the SODA. Even though there are differences between the reanalyses, they all depict a similar relationship between ENSO and TT to the results shown by Sobel et al. (2002).

Spatially the correlations between the AWP area and the TT anomalies are the same in all three lead−lag relationships in all three reanalyses. In the contemporaneous correlation (Figures 3.34a, 3.35a, and 3.36a), there are positive correlations seen throughout the global tropical troposphere with correlation values between 0.5 and 0.7 in the tropical Atlantic. However, three months after (NDJ) (Figures 3.34b, 3.35b, and 3.36b) and six months after (FMA) (Figures 3.34c, 3.35c, and 3.36c), the global tropical troposphere is not warmed. Three months after (NDJ), there are no positive correlations seen in the central and eastern Pacific for any of the three reanalyses, and the correlation values in tropical Atlantic are lower with values between 0.381 and 0.5. Additionally, the SODA shows no correlations in the northern Indian Ocean. Six months after (FMA), the reanalyses show positive correlations in the western Pacific. Additionally, the CFSR is the only reanalysis with positive correlations in the eastern tropical Atlantic with values between 0.381 and 0.5. This may be due to the fact that CFSR is a coupled reanalysis and is better at capturing the interaction between the ocean and the atmosphere. However, this is speculation and should be further examined.

In all three reanalyses, the AWP does not warm the global tropical troposphere three to six months after. However, the global tropical troposphere is warmed contemporaneously (ASO). The signal slowly disappears three months (NDJ) and six months after (FMA), however, this is merely speculation and should be further studied.

As just summarized, for all three reanalyses, the AWP exhibits a seasonal cycle. In addition, the AWP area is affected by global SSTs, as well as by subsurface ocean temperatures throughout the Atlantic Ocean basin. The evolution of the AWP is greatly affected by surface heat fluxes through a negative relationship in that the fluxes cause the AWP to shrink. Small AWPs have a higher hurricane heat potential compared to large AWPs. Advective terms play a role in expanding and contracting the AWP throughout the year. Futthermore, the AWP does not cause the global tropical troposphere to warm three to six months after the AWP is at a maximum (ASO).

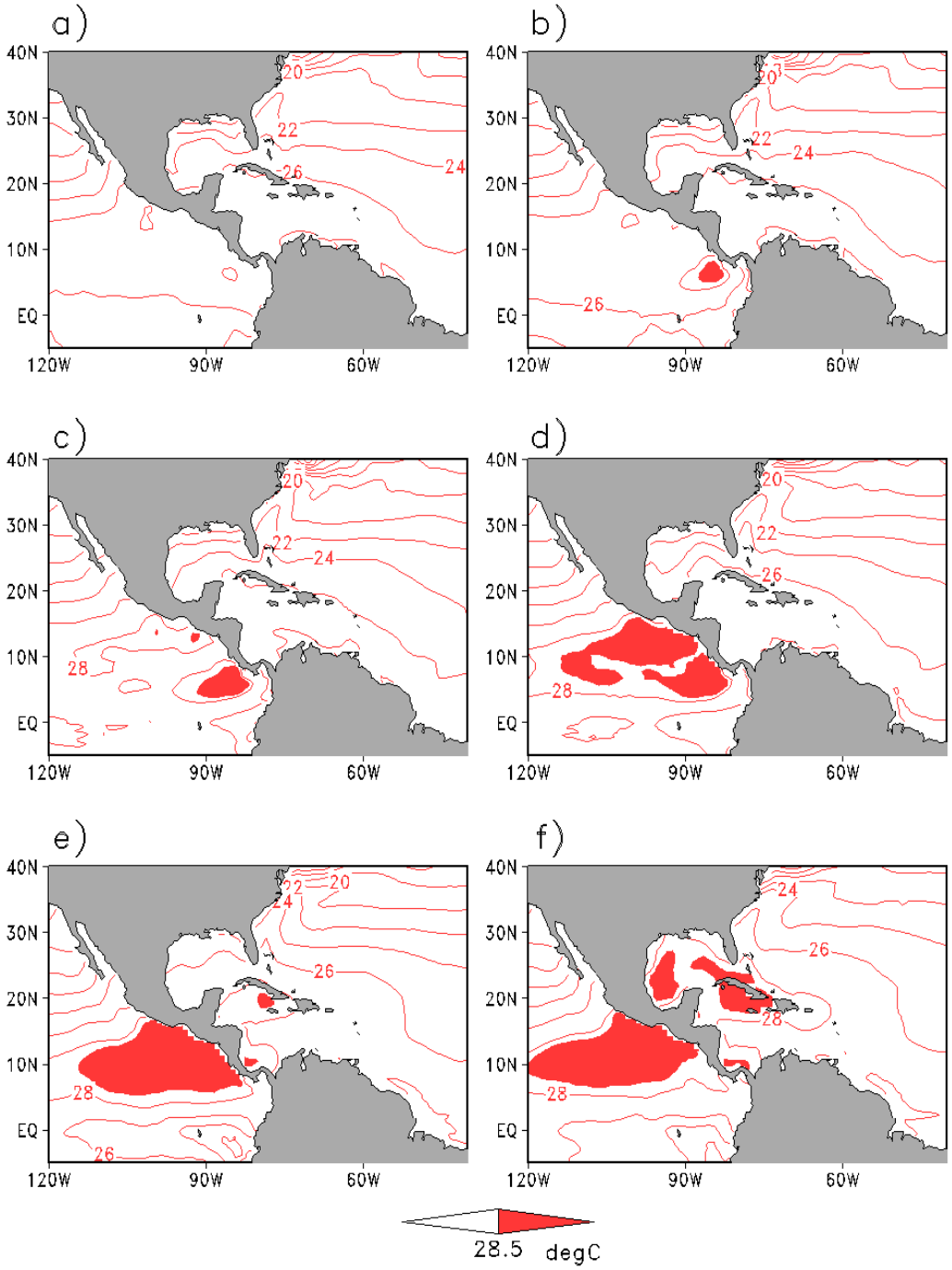


Figure 3.1. Monthly mean of SSTs (°C) in GODAS: a) January, b) February, c) March, d) April, e) May, and f) June. SSTs are contoured and SSTs greater than 28.5°C are shaded in red.

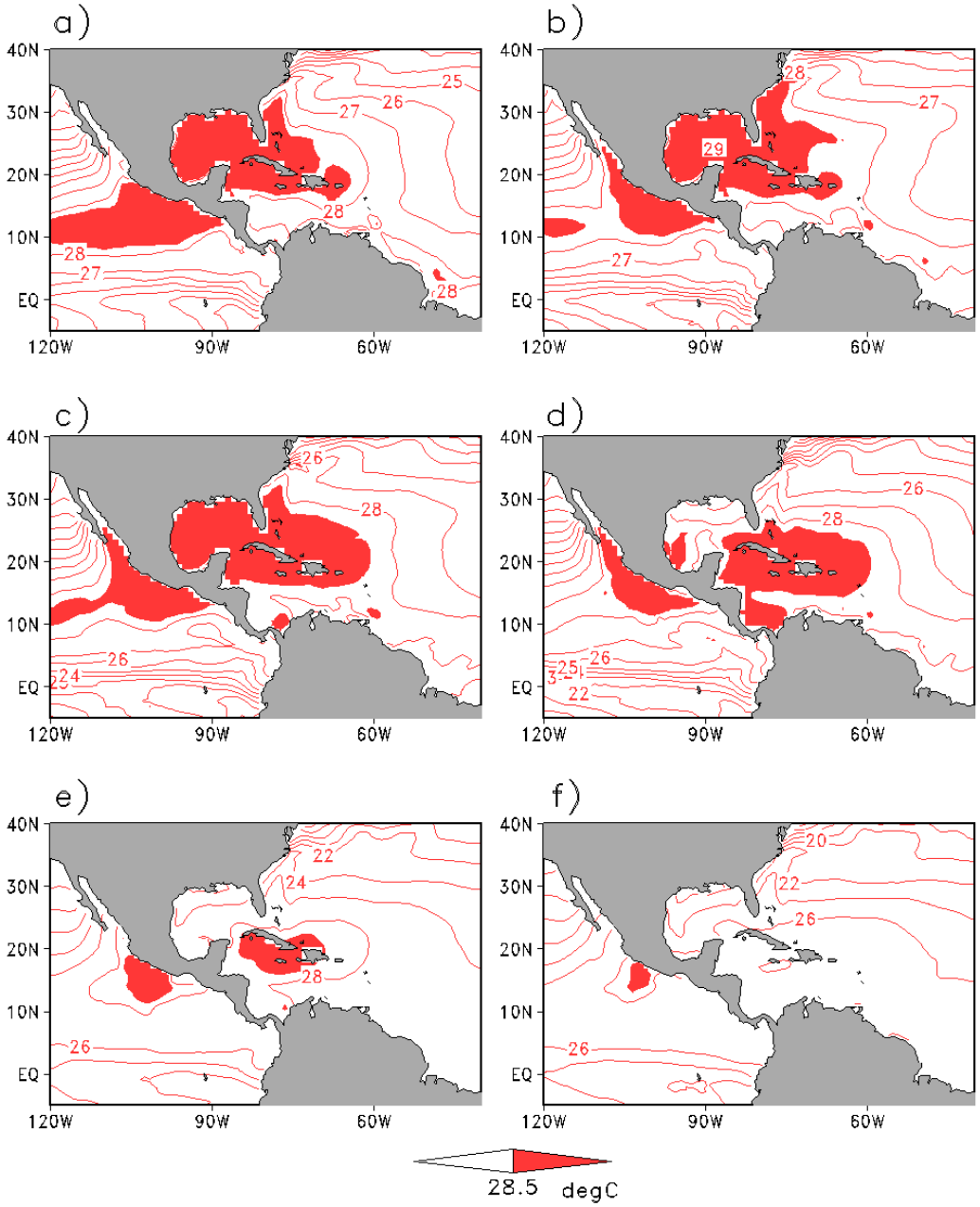


Figure 3.2. Monthly mean of SSTs (°C ) in GODAS: a) July, b) August, c) September, d) October, e) November, and f) December. SSTs are contoured and SSTs greater than 28.5°C are shaded in red.

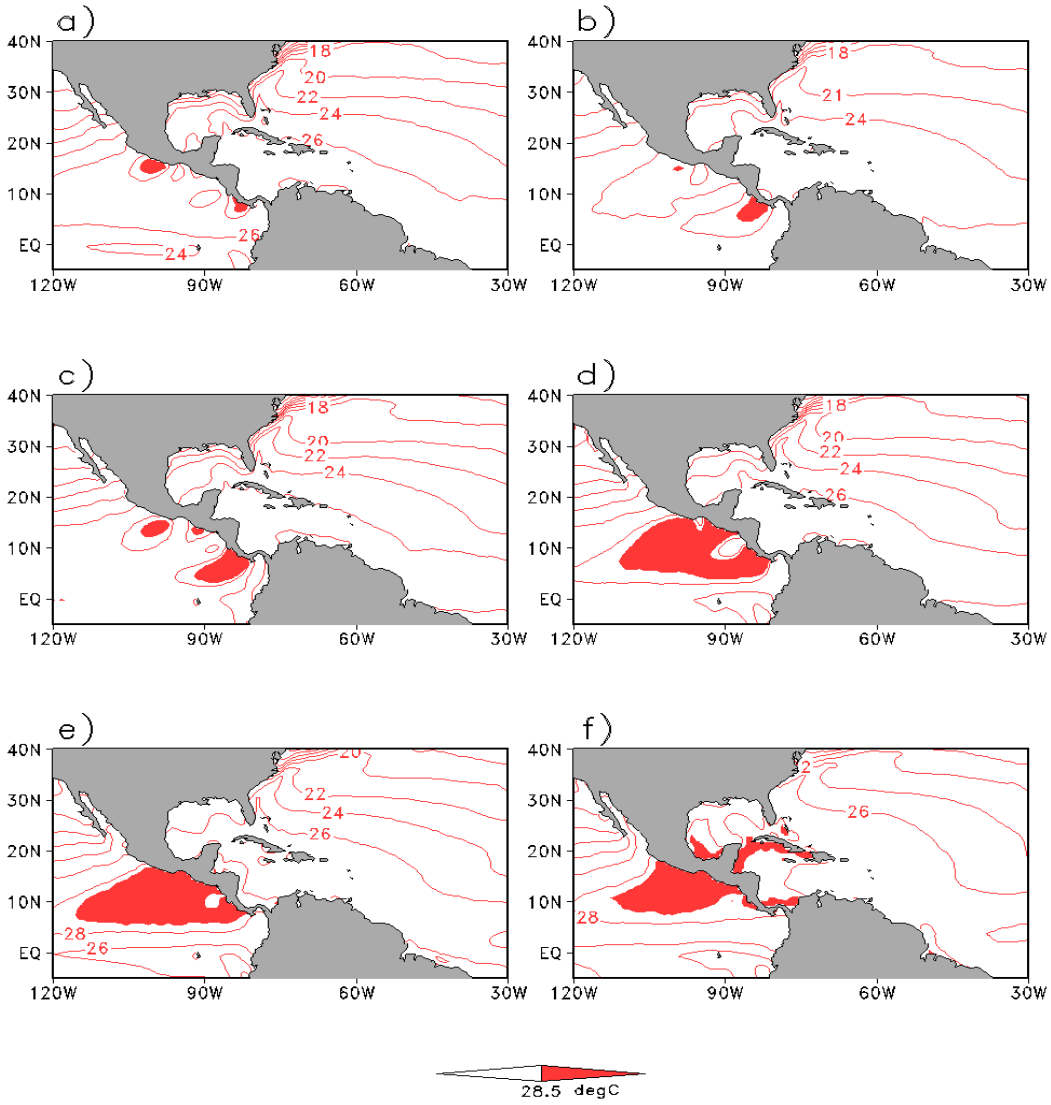


Figure 3.3. Same as Figure 3.1 but for CFSR.

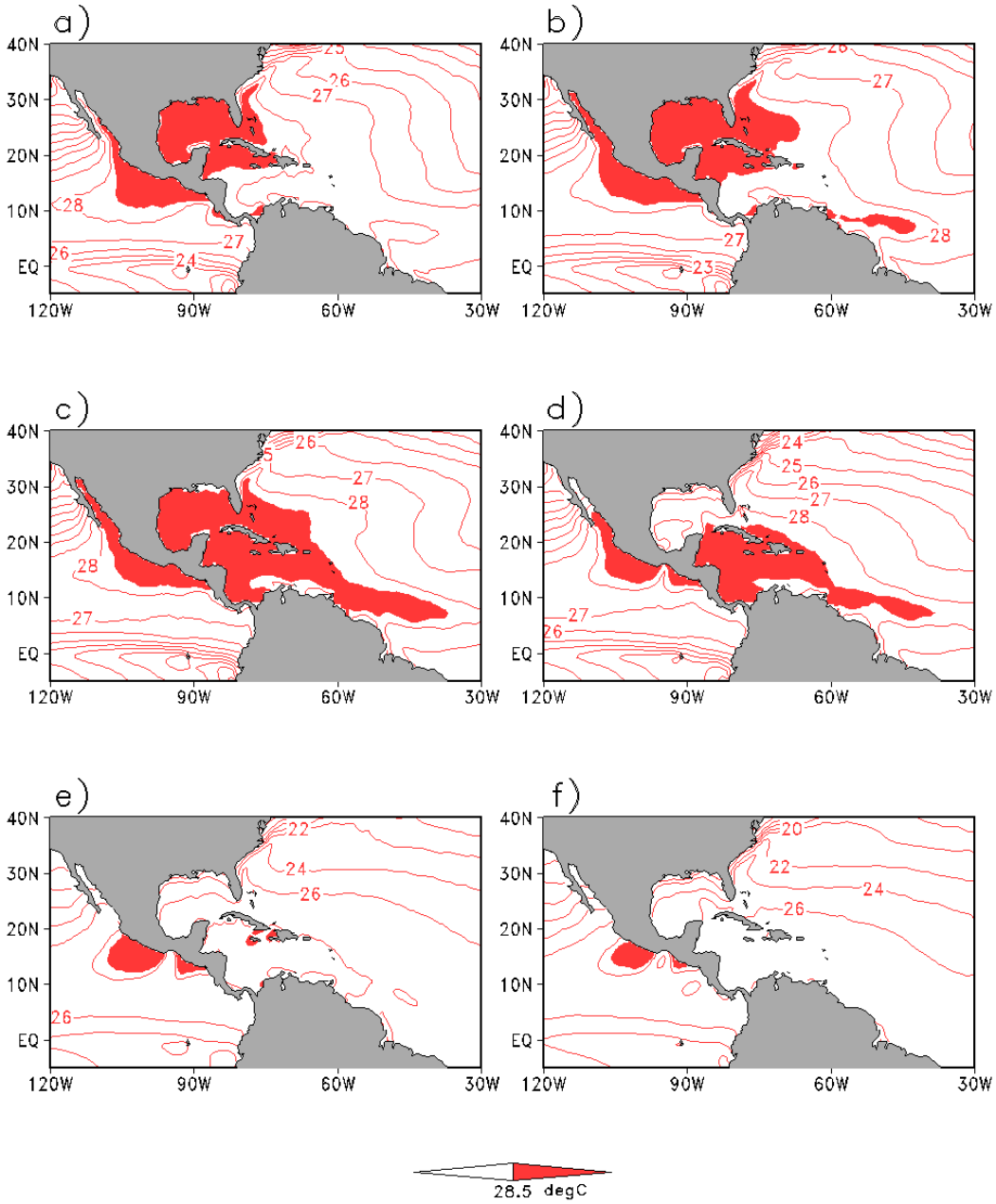


Figure 3.4. Same as Figure 3.2 but for CFSR.

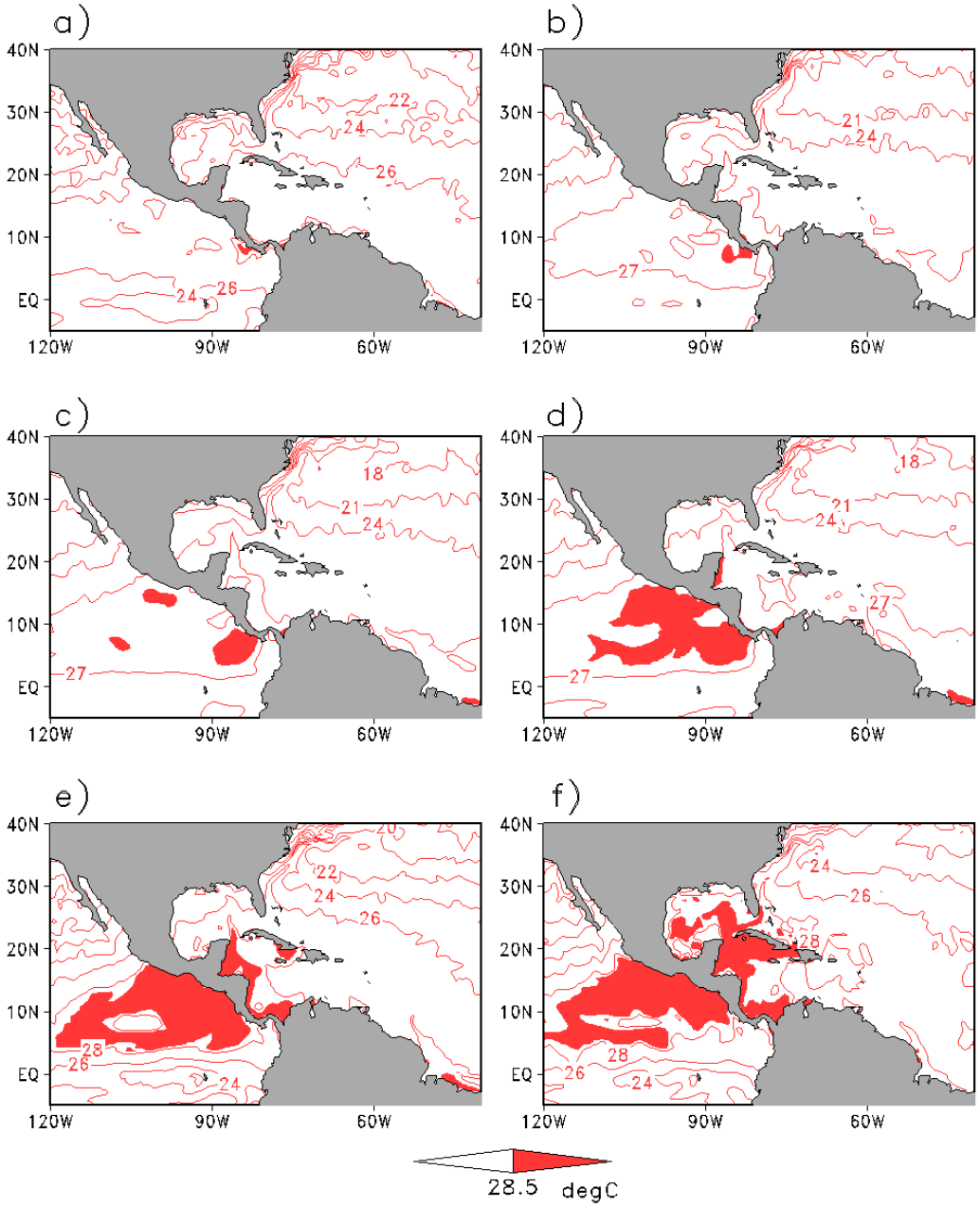


Figure 3.5. Same as Figure 3.1 but for SODA.

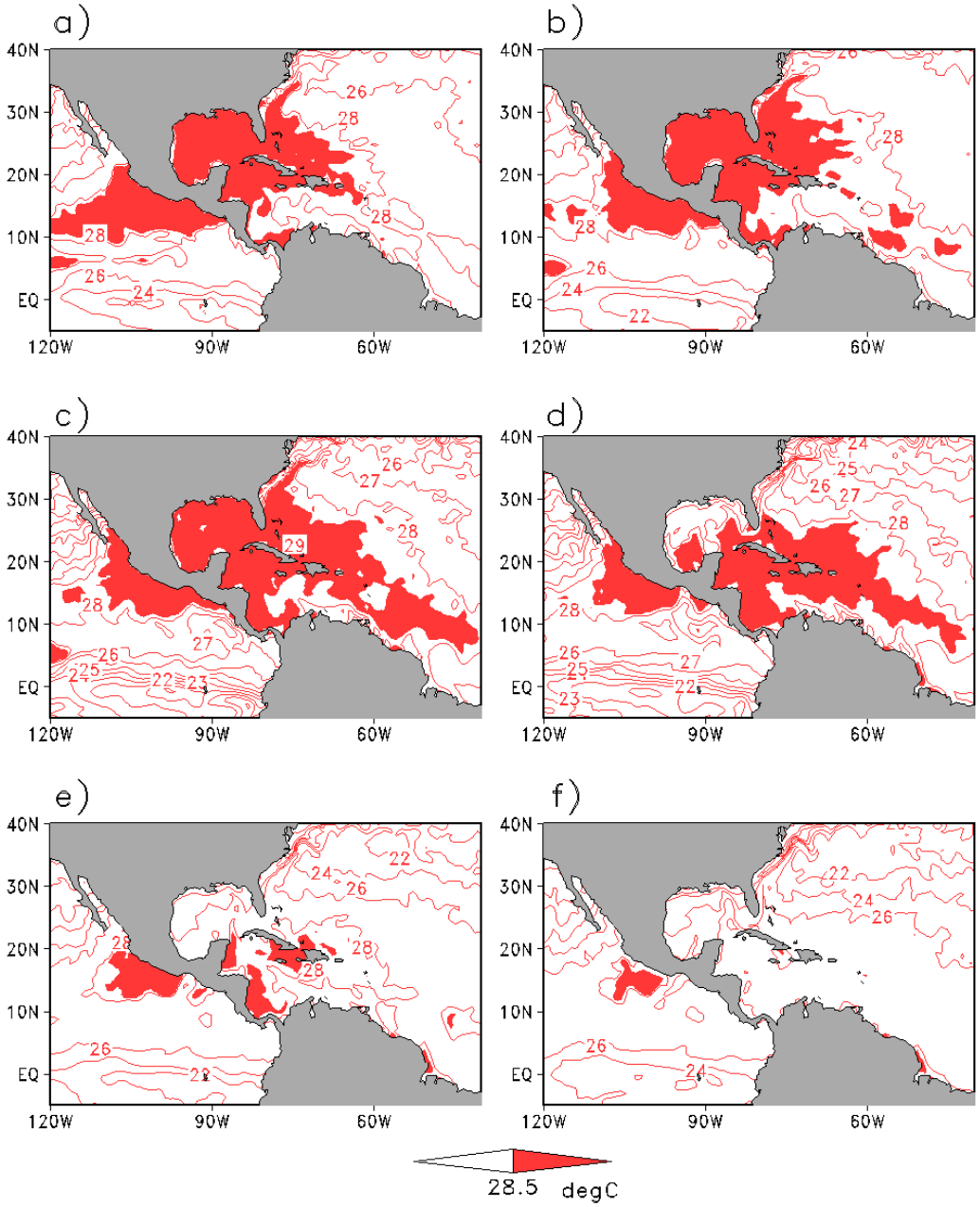


Figure 3.6. Same as Figure 3.2 but for SODA.

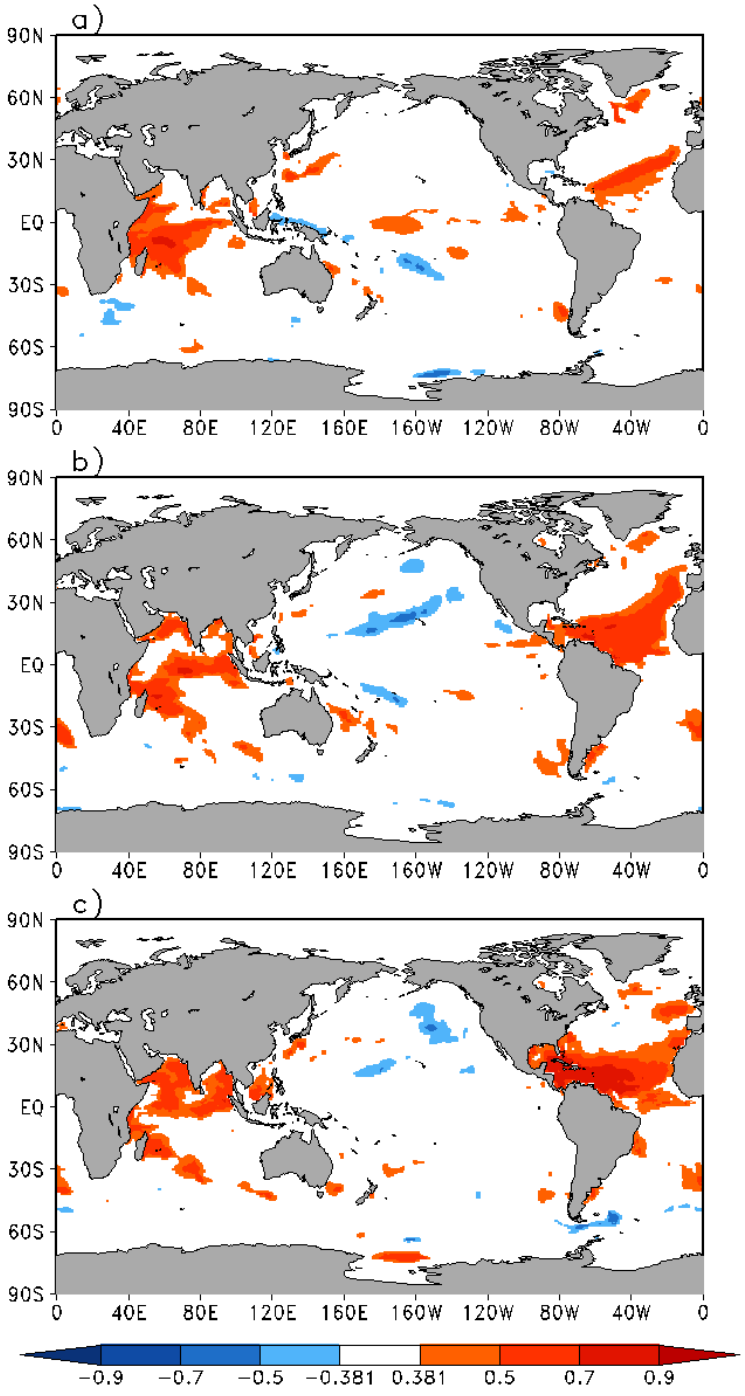


Figure 3.7. Correlation of ASO AWP area with the a) FMA SSTAs, b) MJJ SSTAs, and c) ASO SSTAs in GODAS. The SSTAs are leading. Only values that are greater than the 95% significance ( $|r| \geq 0.381$) are shown.

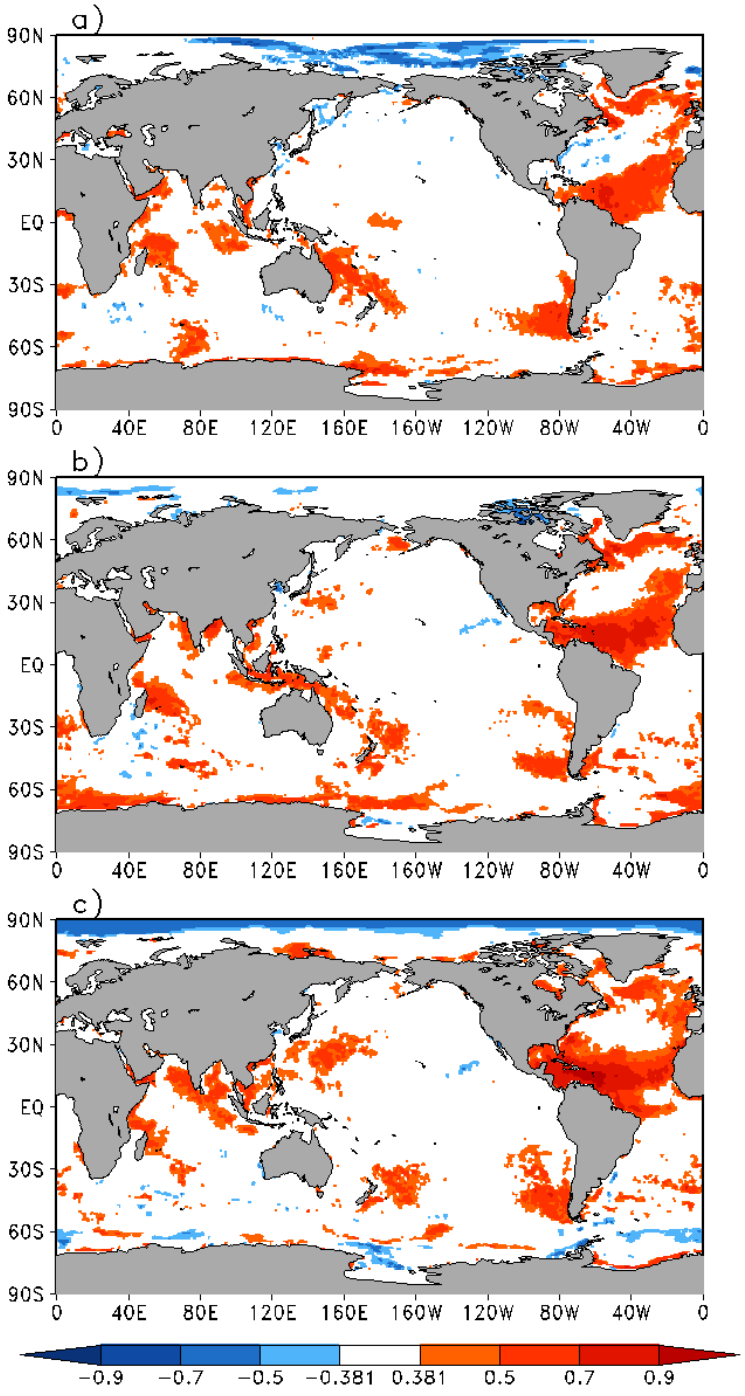


Figure 3.8. Same as Figure 3.7 but for CFSR.

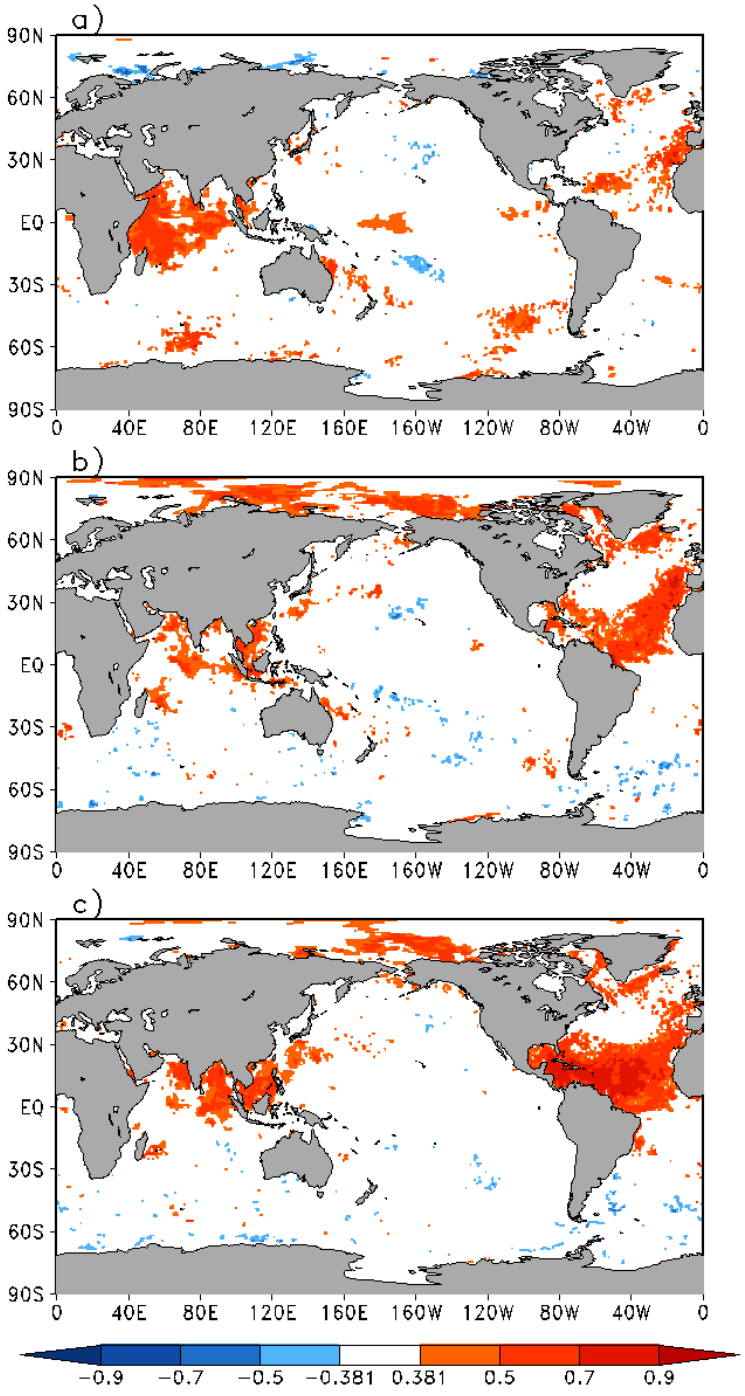


Figure 3.9. Same as Figure 3.7 but for SODA.

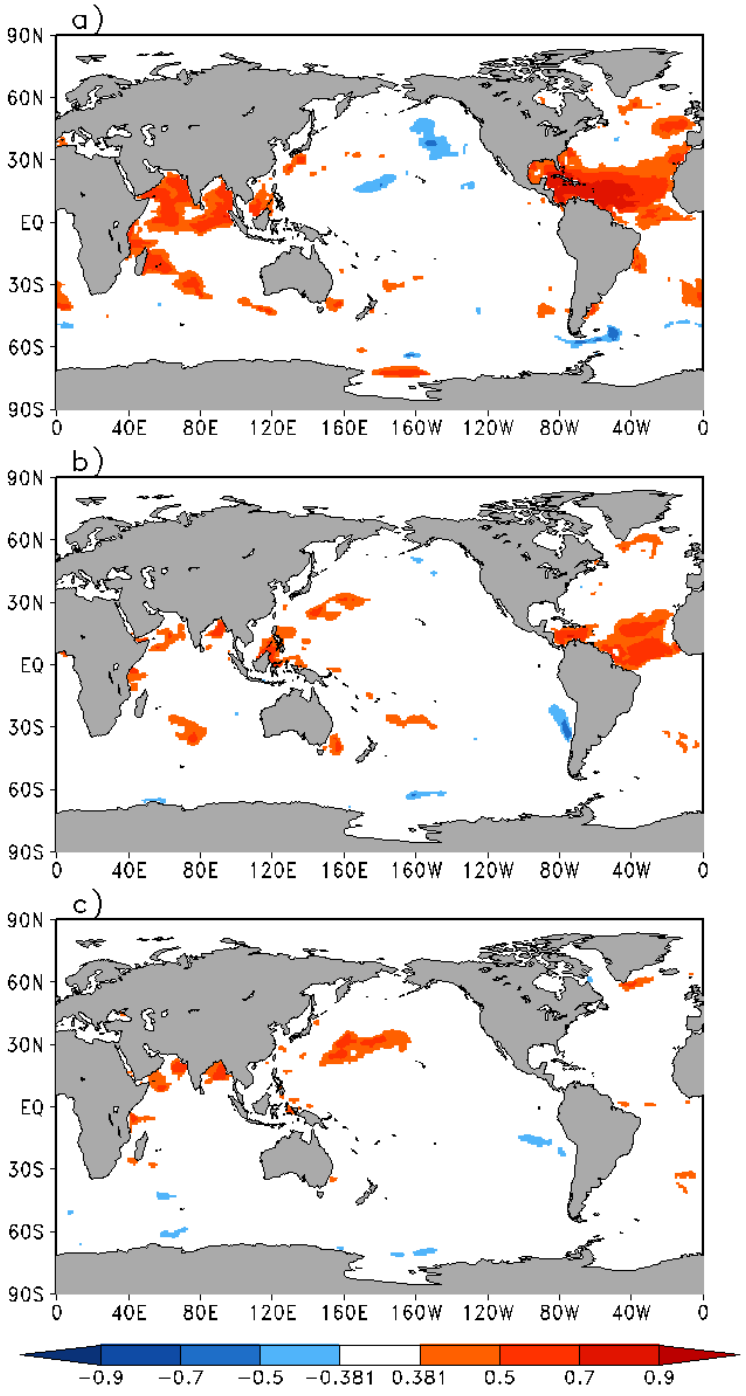


Figure 3.10. Correlation of ASO AWP area with the a) ASO SSTAs, b) NDJ SSTAs, and c) FMA SSTAs in GODAS. The AWP area is leading. Only values that are greater than the 95% significance ( $|r| \geq 0.381$) are shown.

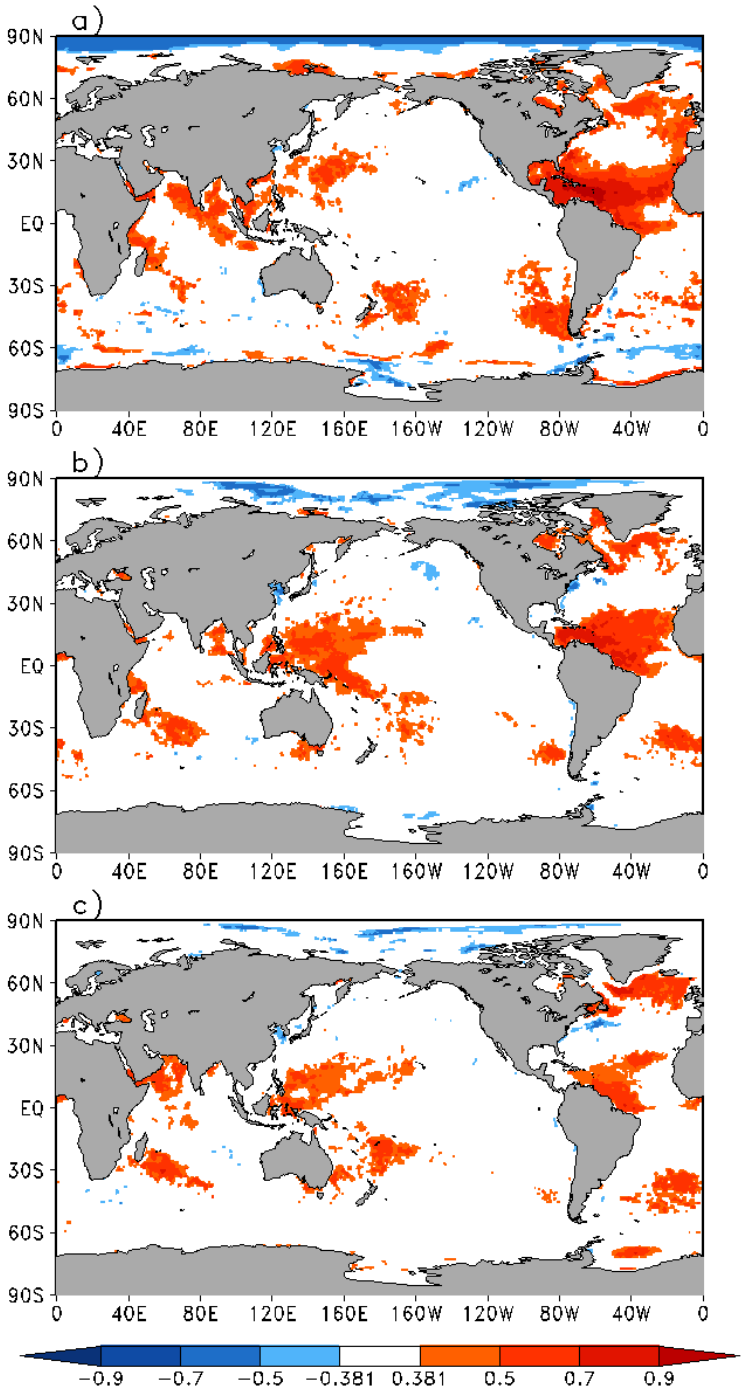


Figure 3.11. Same as Figure 3.10 but for CFSR.

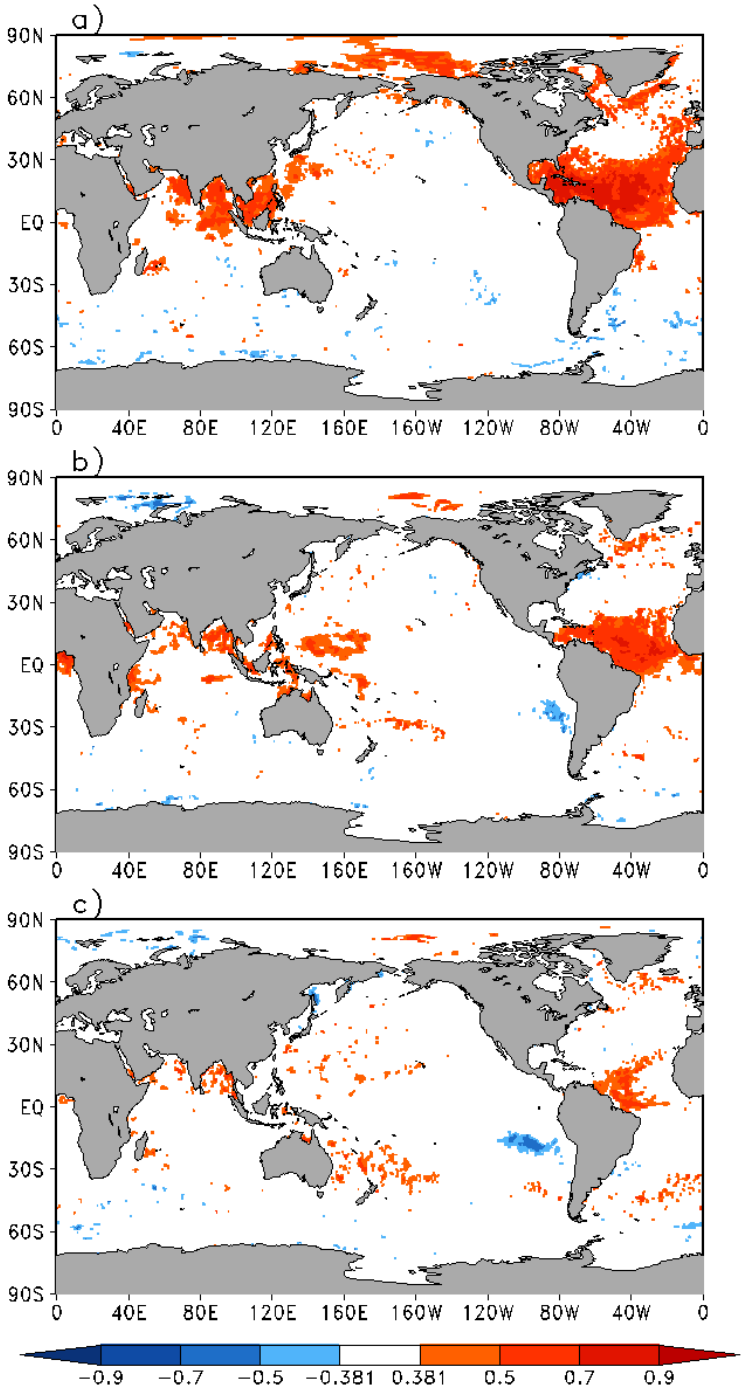


Figure 3.12. Same as Figure 3.10 but for SODA.

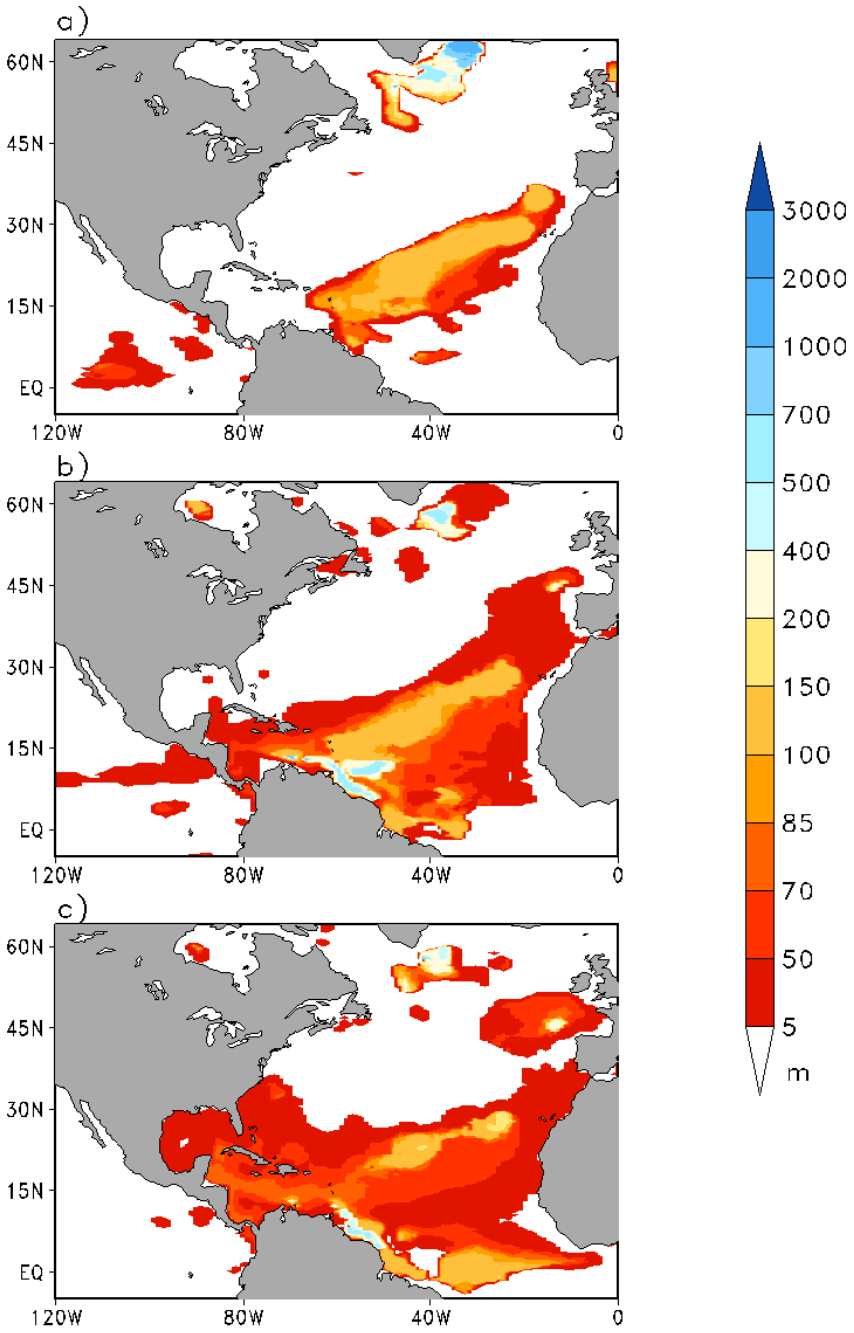


Figure 3.13. Depth at which correlations of the ASO AWP area with the a) FMA STAs, b) MJJ STAs, and c) ASO STAs are no longer significant in GODAS. The STAs are leading. . Only values that are greater than the 95% significance ( $|r| \geq 0.381$) are shown.

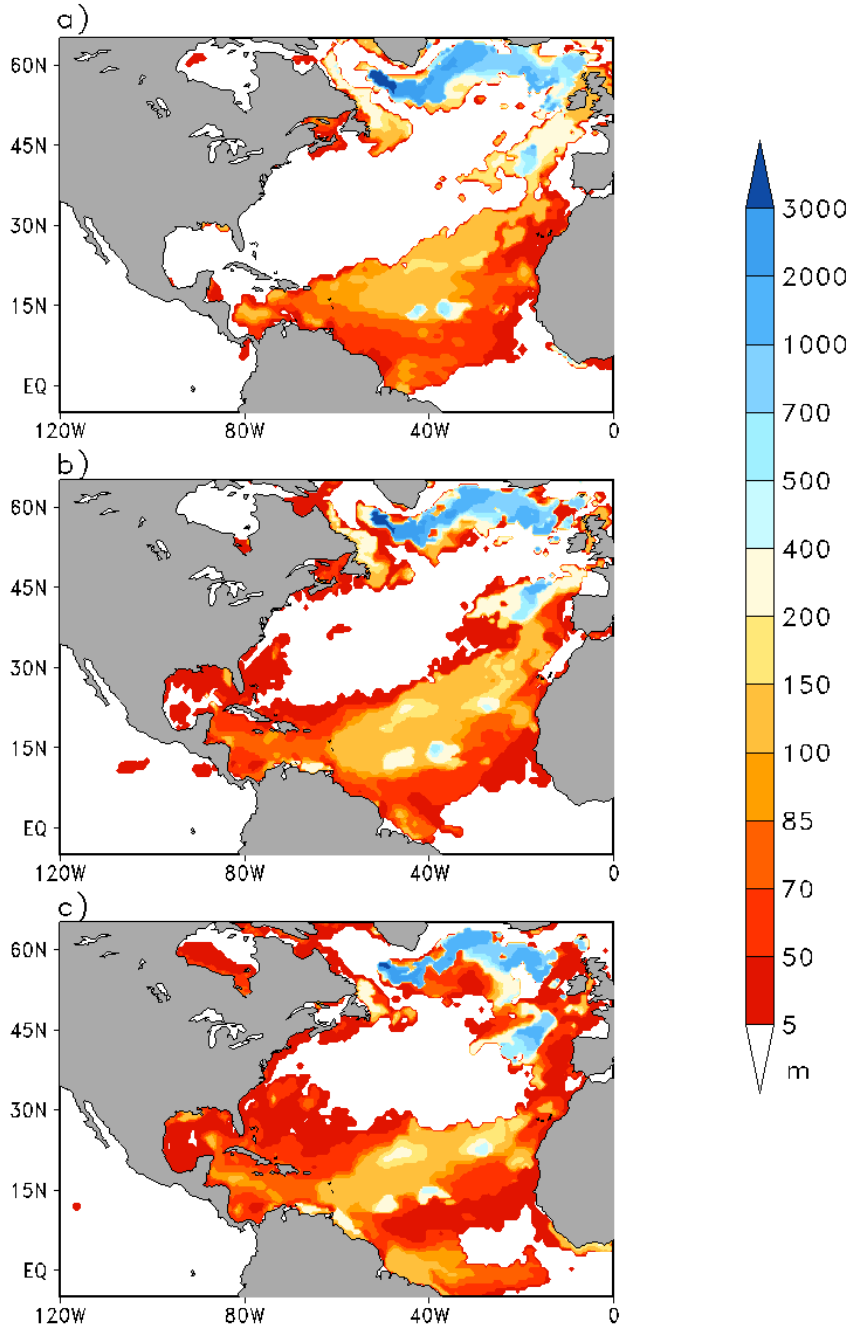


Figure 3.14. Same as Figure 3.13 but for CFSR.

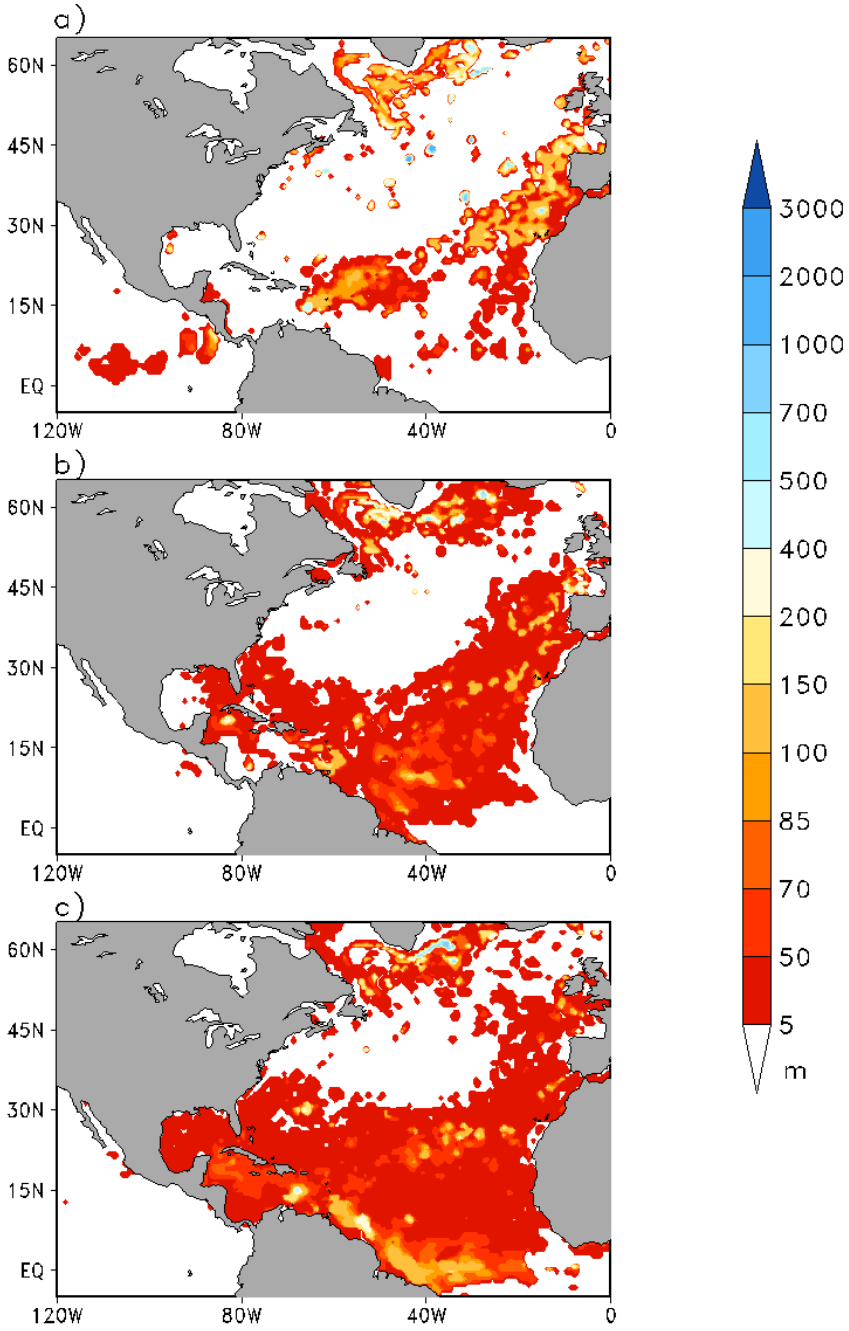


Figure 3.15. Same as Figure 3.13 but for SODA.

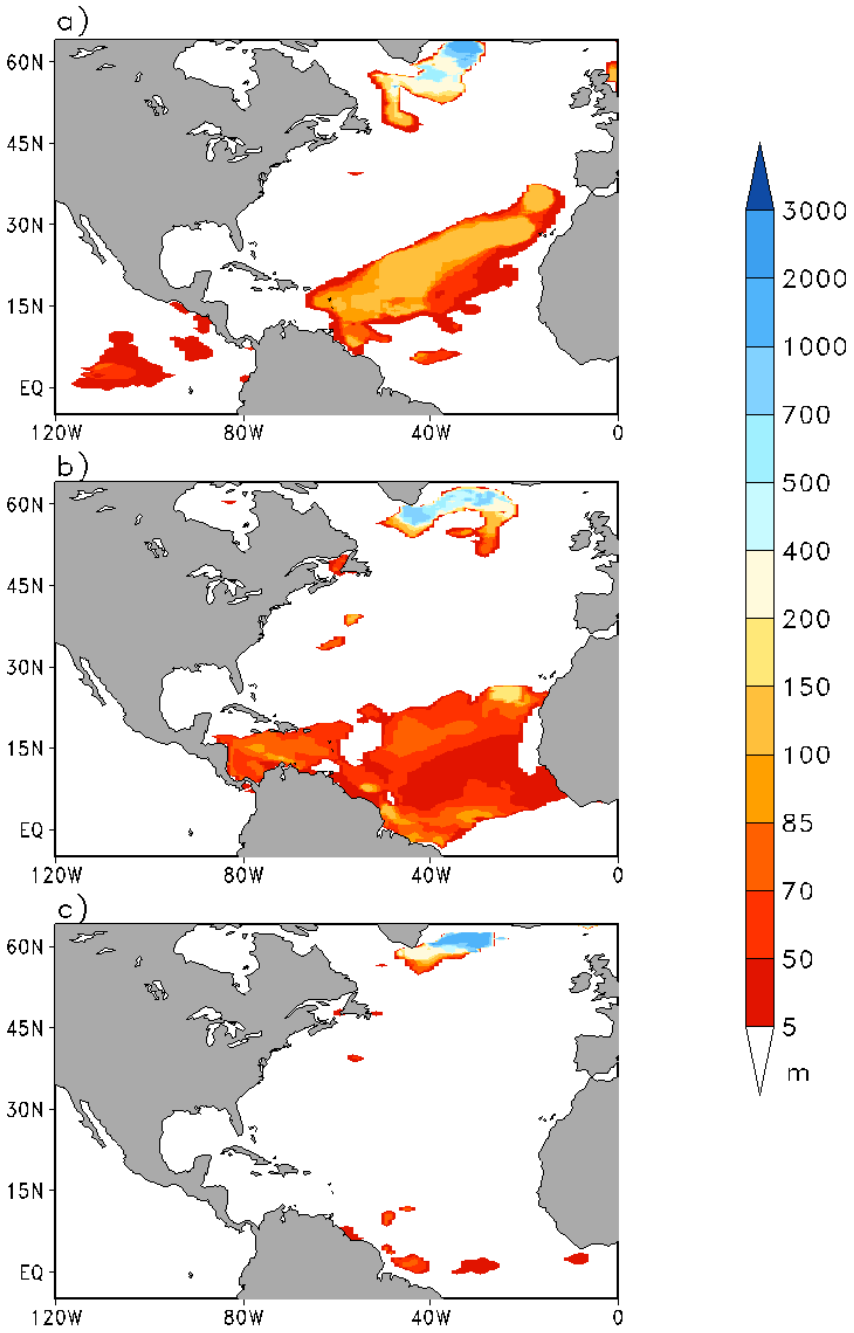


Figure 3.16. Depth at which correlations of the ASO AWP area with the a) ASO STAs, b) NDJ STAs, and c) FMA STAs are no longer significant in GODAS. The AWP area is leading. . Only values that are greater than the 95% significance ( $|r| \geq 0.381$) are shown.

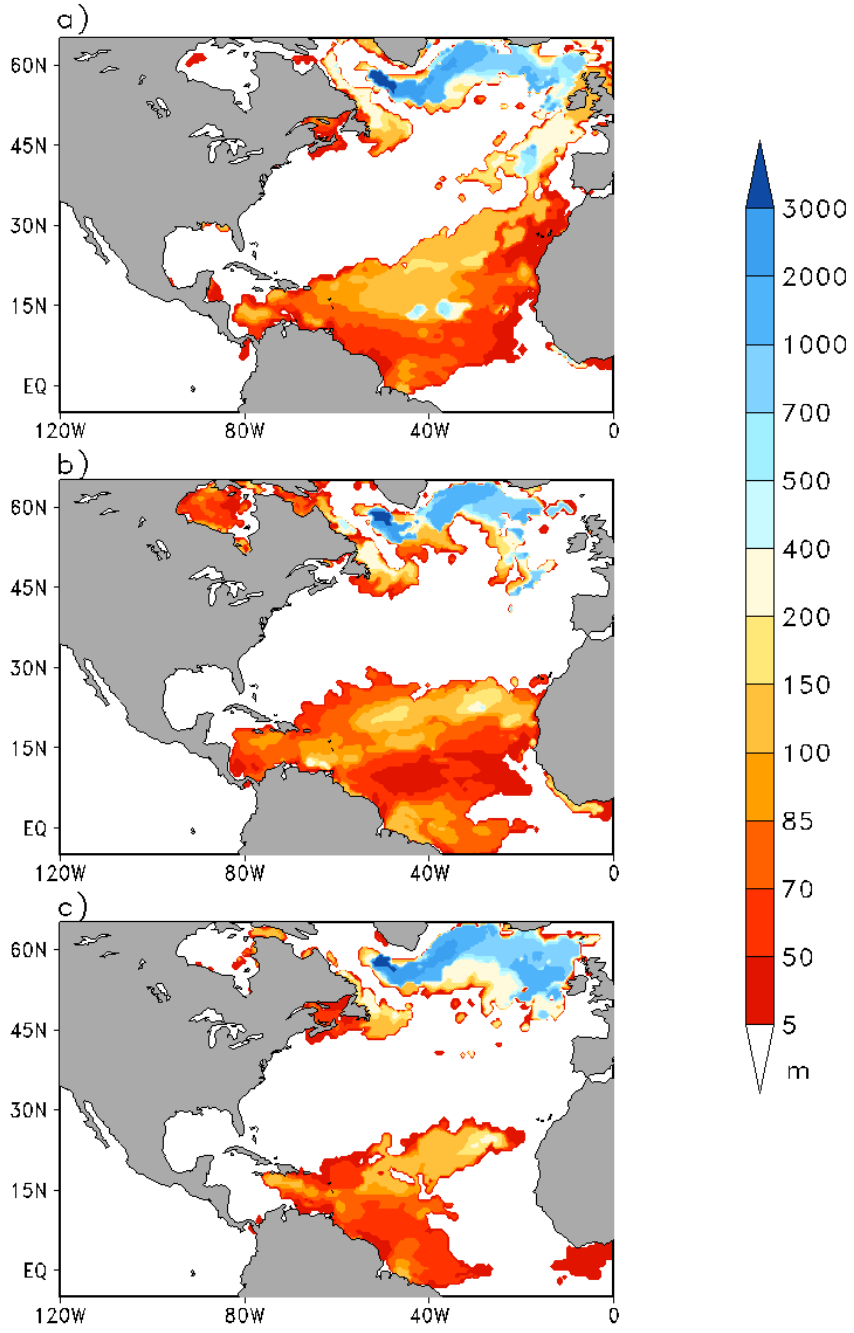


Figure 3.17. Same as Figure 3.16 but for CFSR.

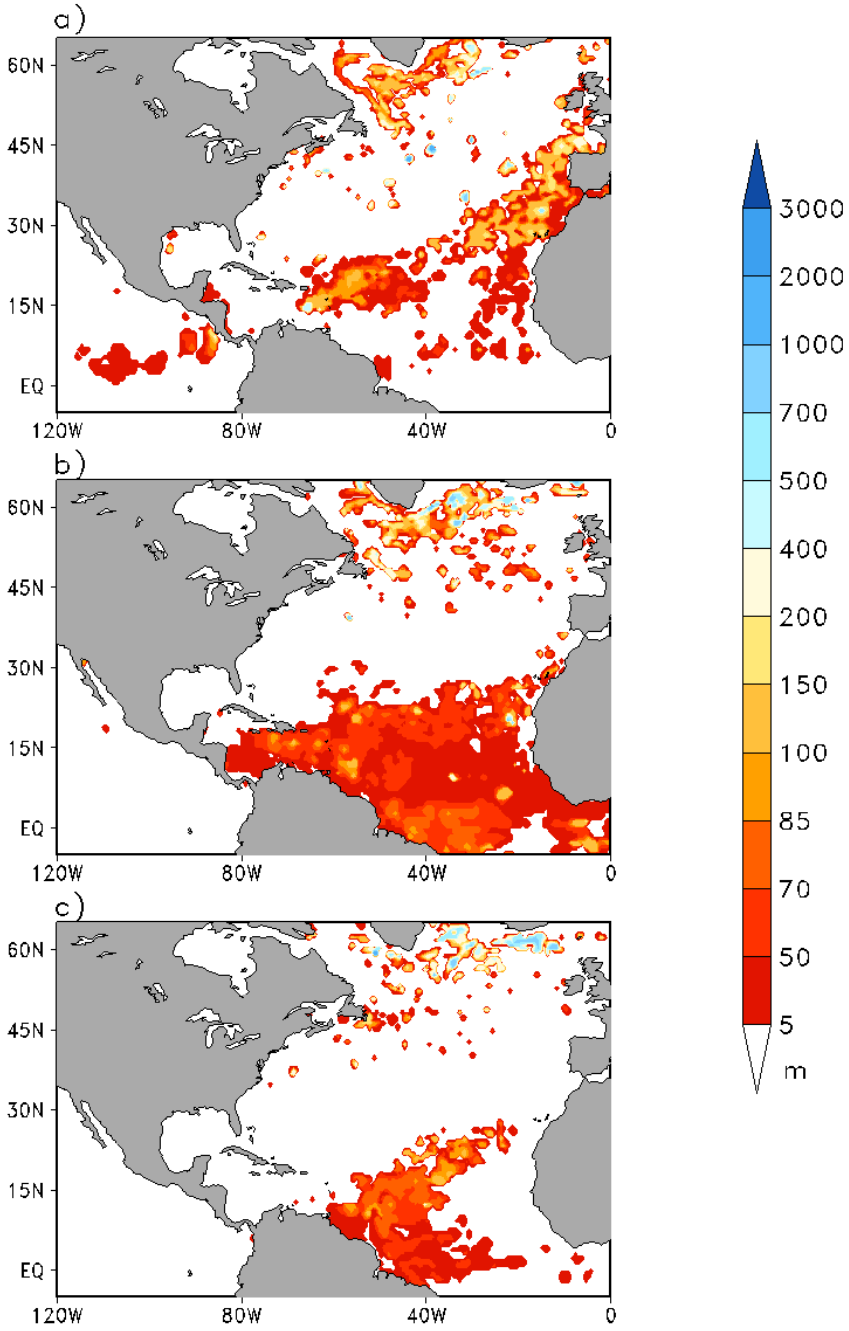


Figure 3.18. Same as Figure 3.16 but for SODA.

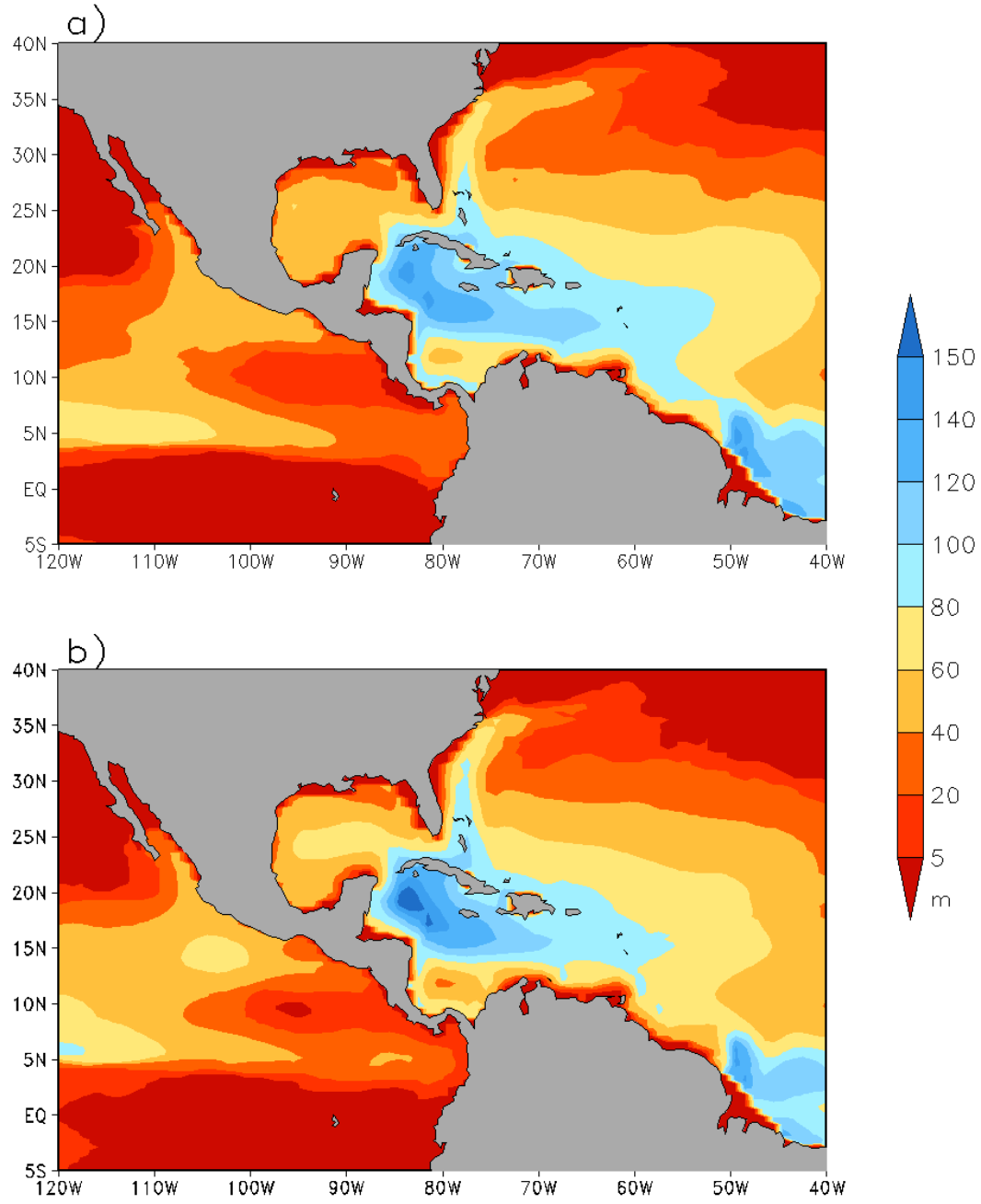


Figure 3.29. Mean depth of the 26.0°C isotherm for the a) five years with the largest AWP area, and b) five years with the smallest AWP area in GODAS. Units of the depth are meters.

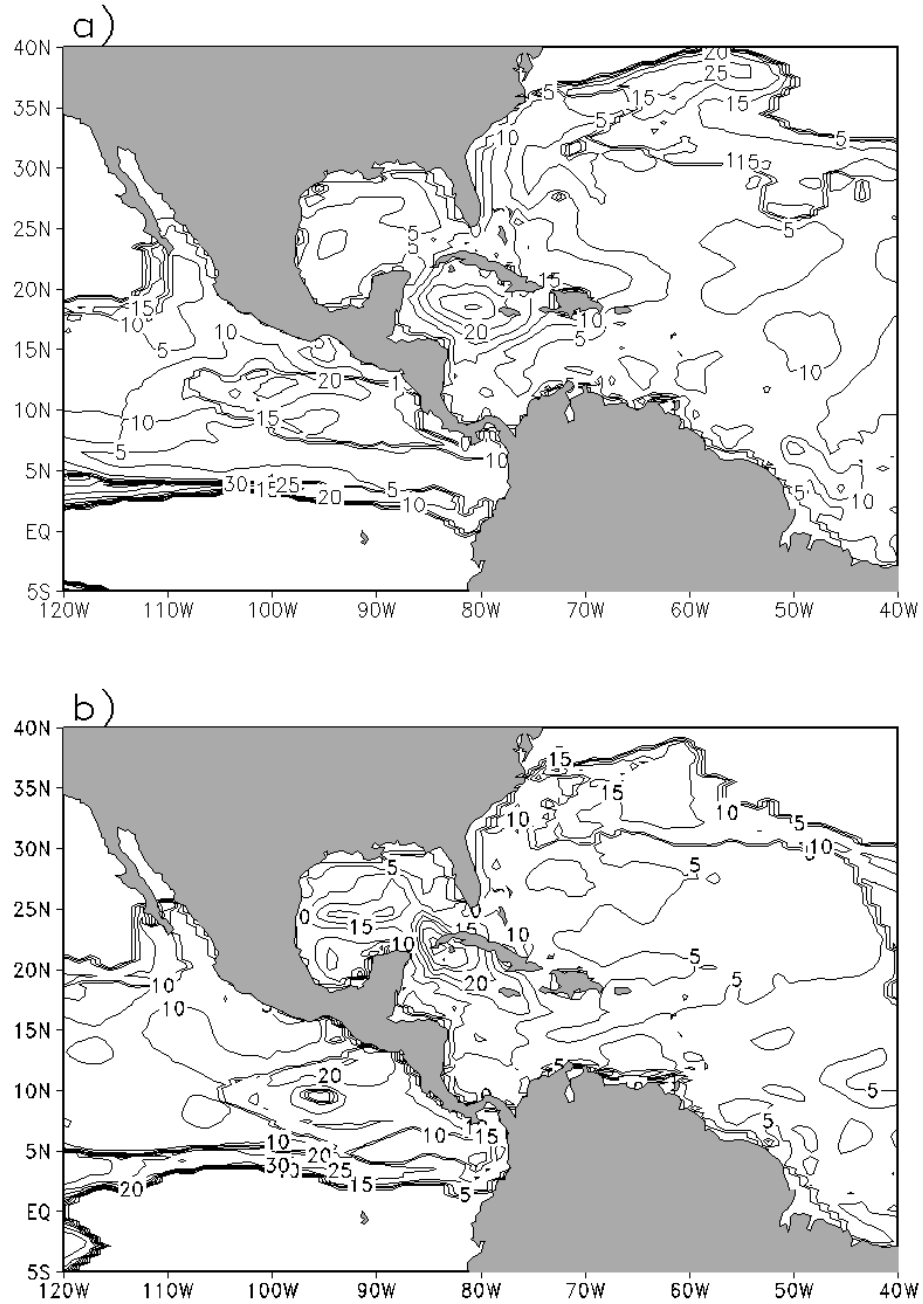


Figure 3.20 Standard Deviation of the mean depth of the 28.5°C isotherm for the a) five years with the largest AWP area, and b) five years with the smallest AWP area in GODAS. Units are meters.

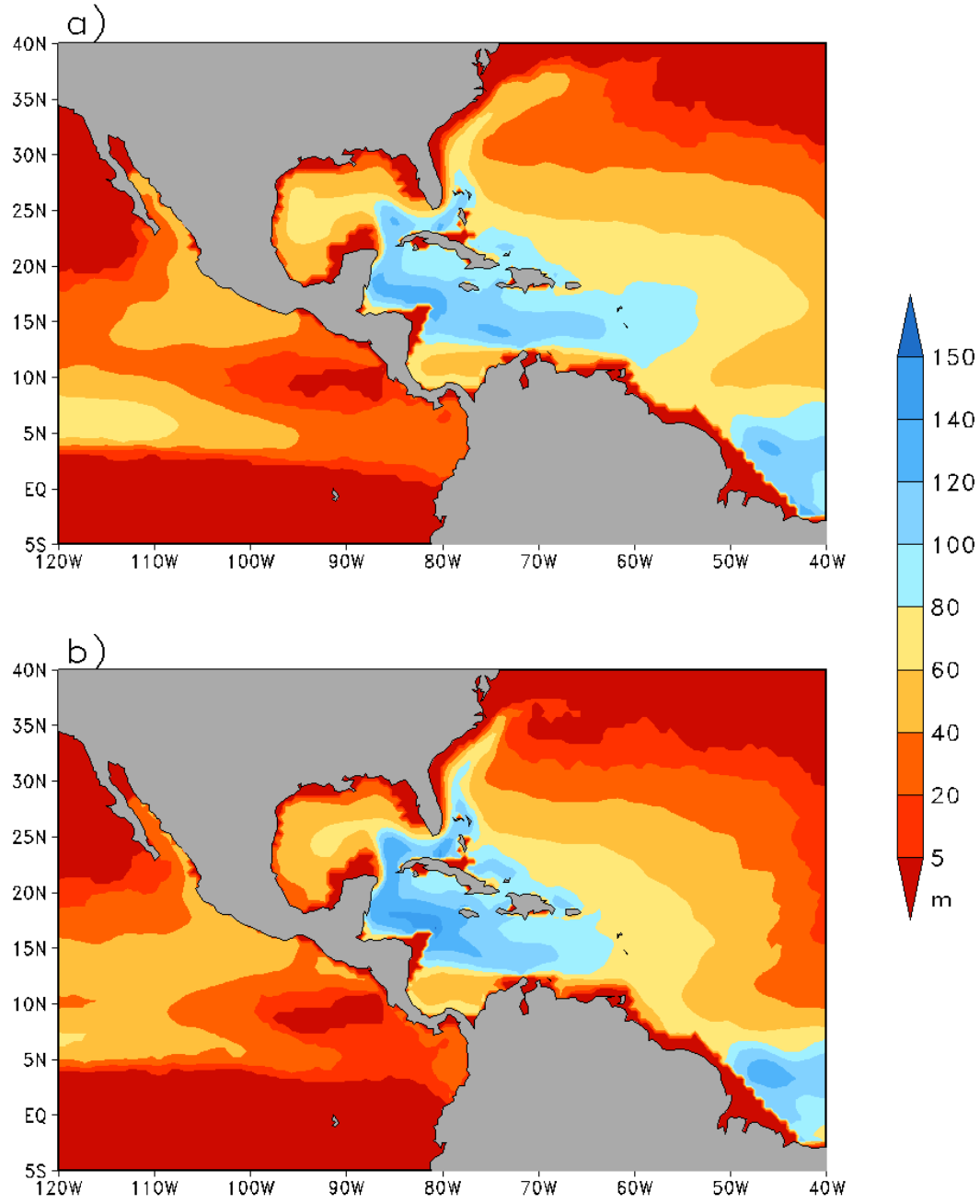


Figure 3.21 Same as Figure 3.19 but for CFSR.

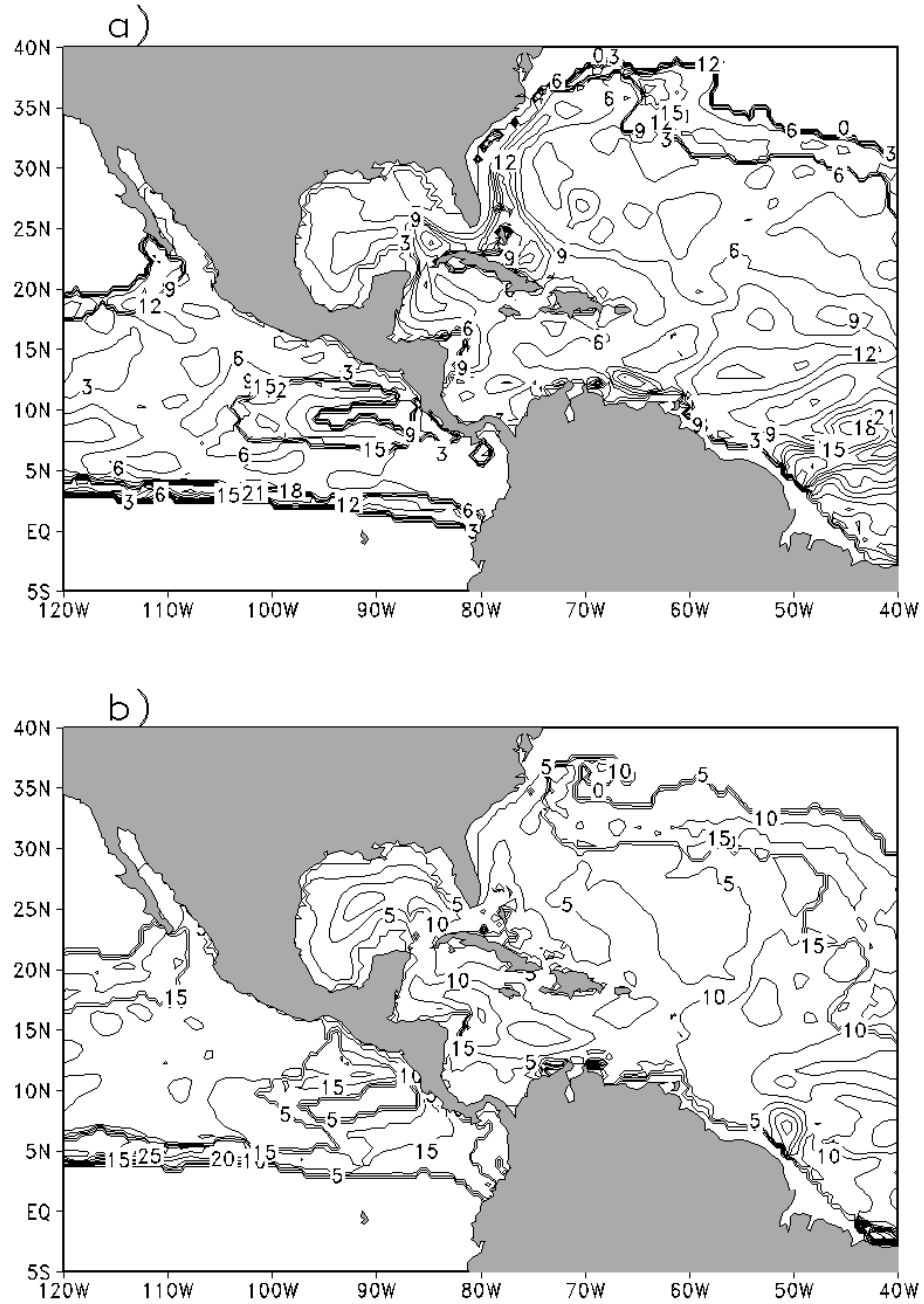


Figure 3.22 Same as Figure 3.20 but for CFSR.

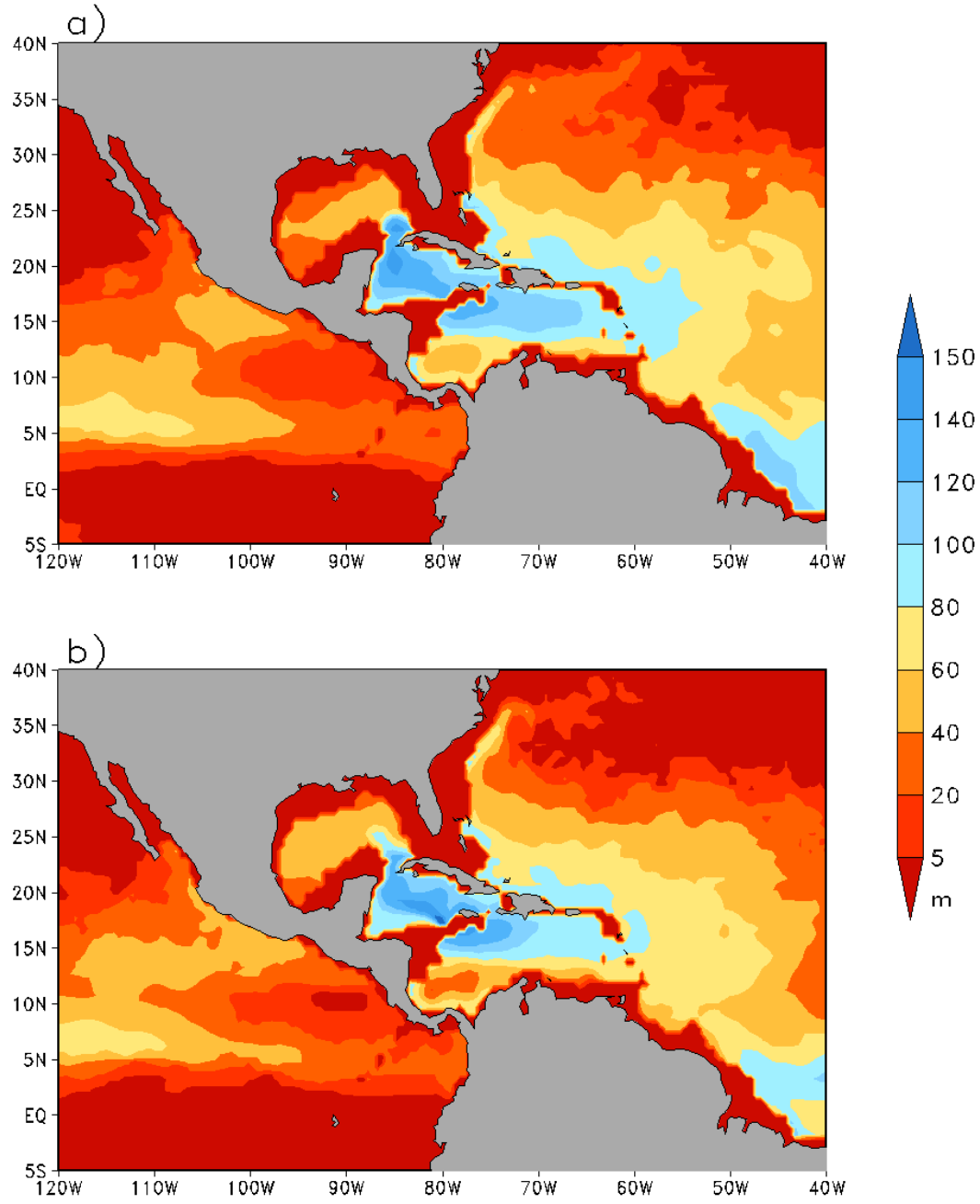


Figure 3.23 Same as Figure 3.19 but for SODA.

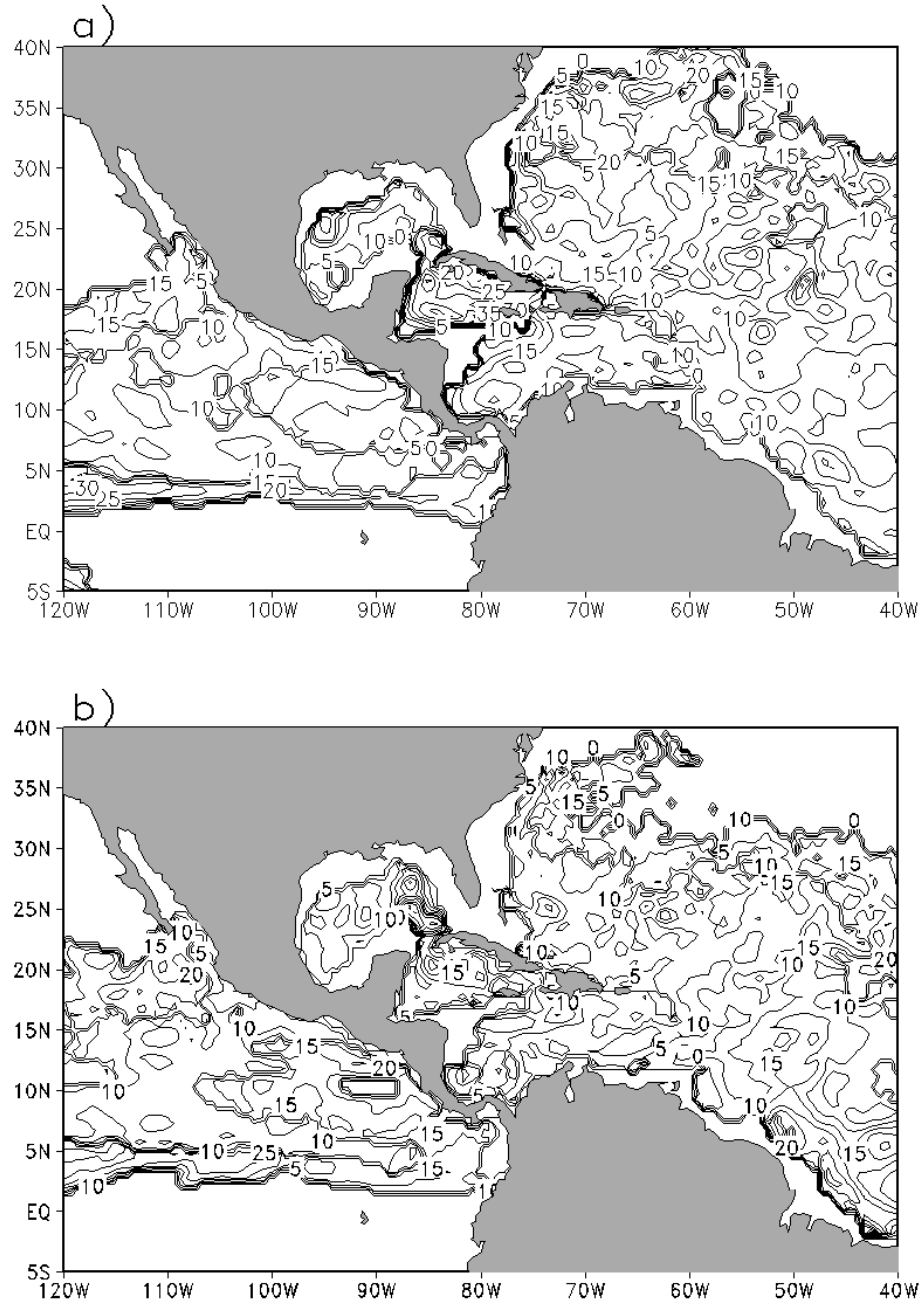


Figure 3.24 Same as Figure 3.20 but for SODA.

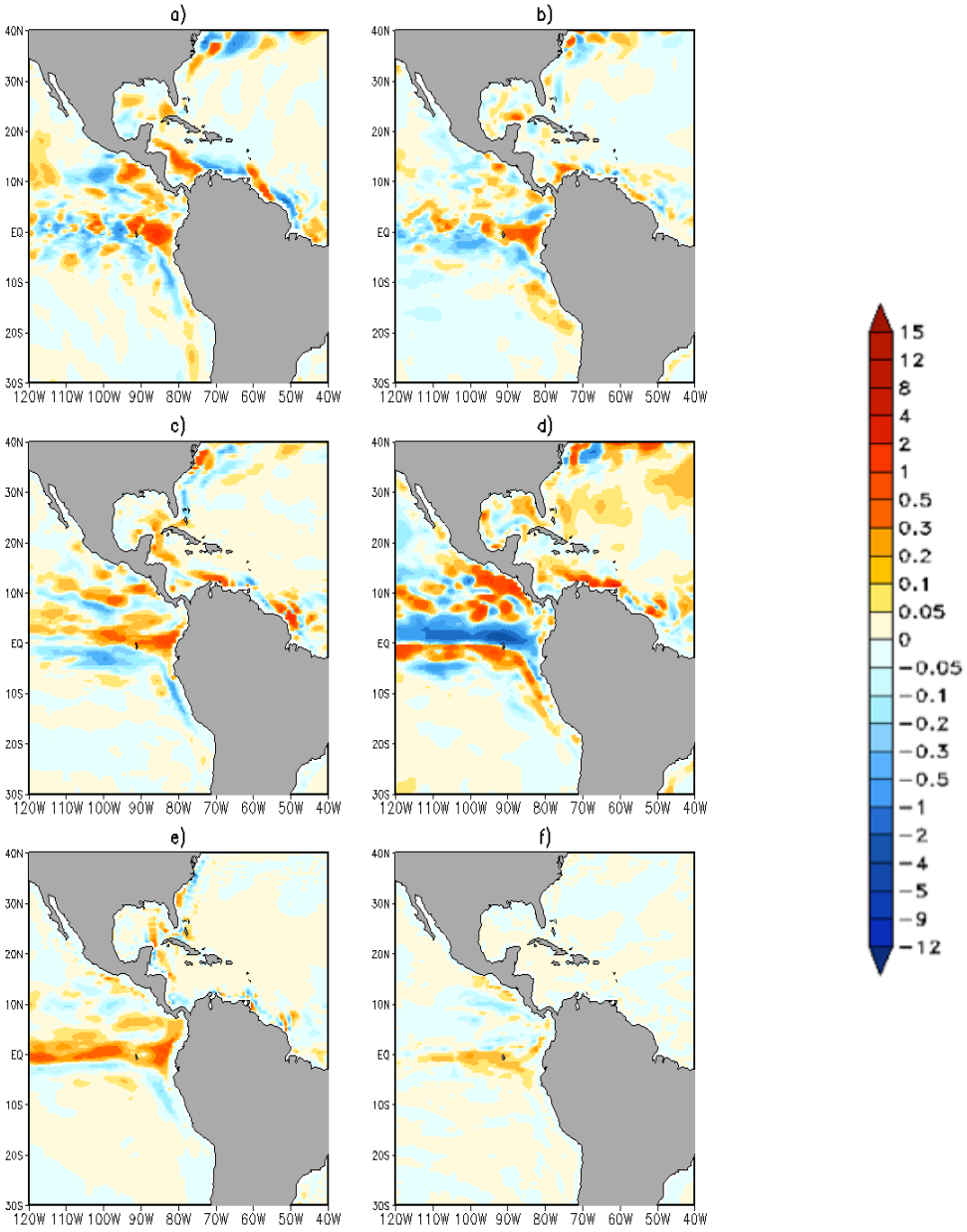


Figure 3.25. Covariance of AWP SST tendency with a) Anomalous temperature advection by the mean zonal current, b) Advection of total temperature by the anomalous zonal current, c) Anomalous temperature advection by the mean meridional current, d) Advection of total temperature by the anomalous meridional current, e) Anomalous temperature advection by the mean vertical current, and f) Advection of total temperature by the anomalous vertical current of the SST anomaly equation normalized by the AWP SST tendency for GODAS.

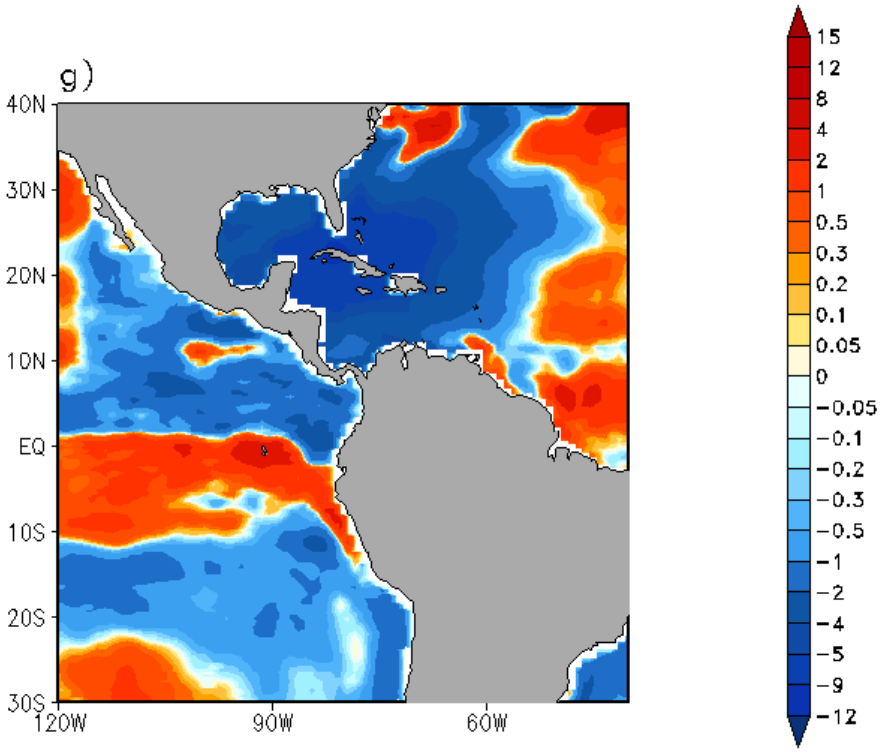


Figure 3.26. Covariance of AWP SST tendency with the anomalous flux term of the SST anomaly equation normalized by the AWP SST tendency for GODAS with R2.

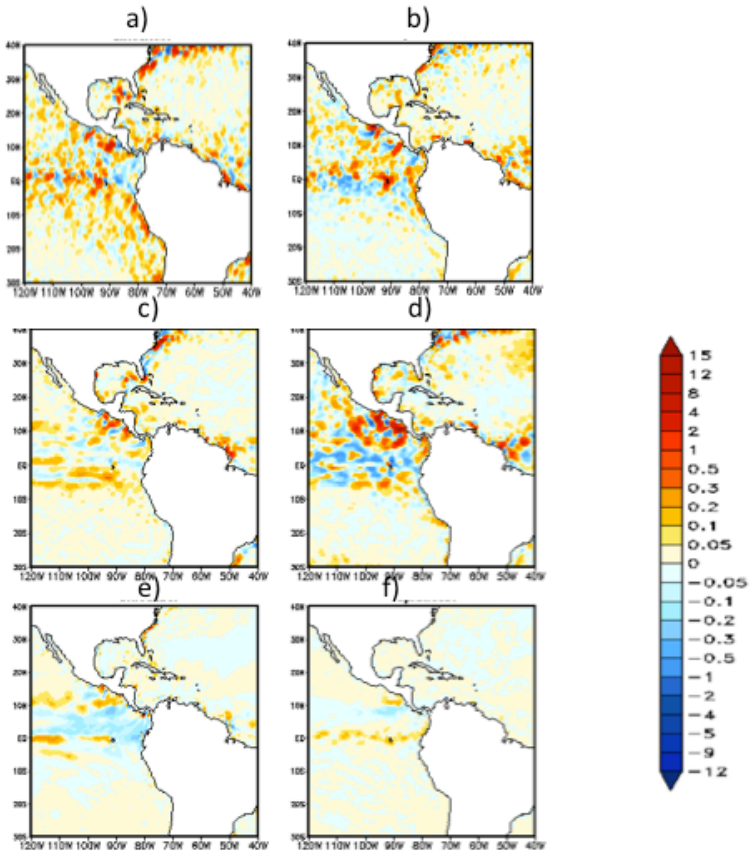


Figure 3.27 Same as Figure 3.25 but for CFSR.

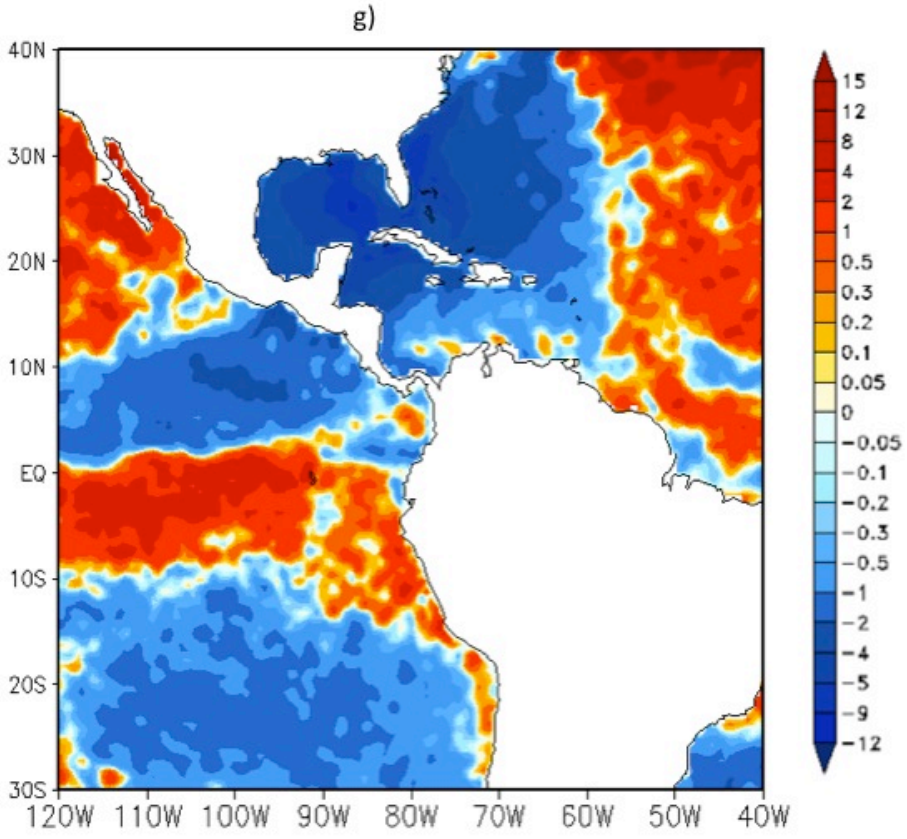


Figure 3.28. Same as Figure 3.26 but for CFSR.

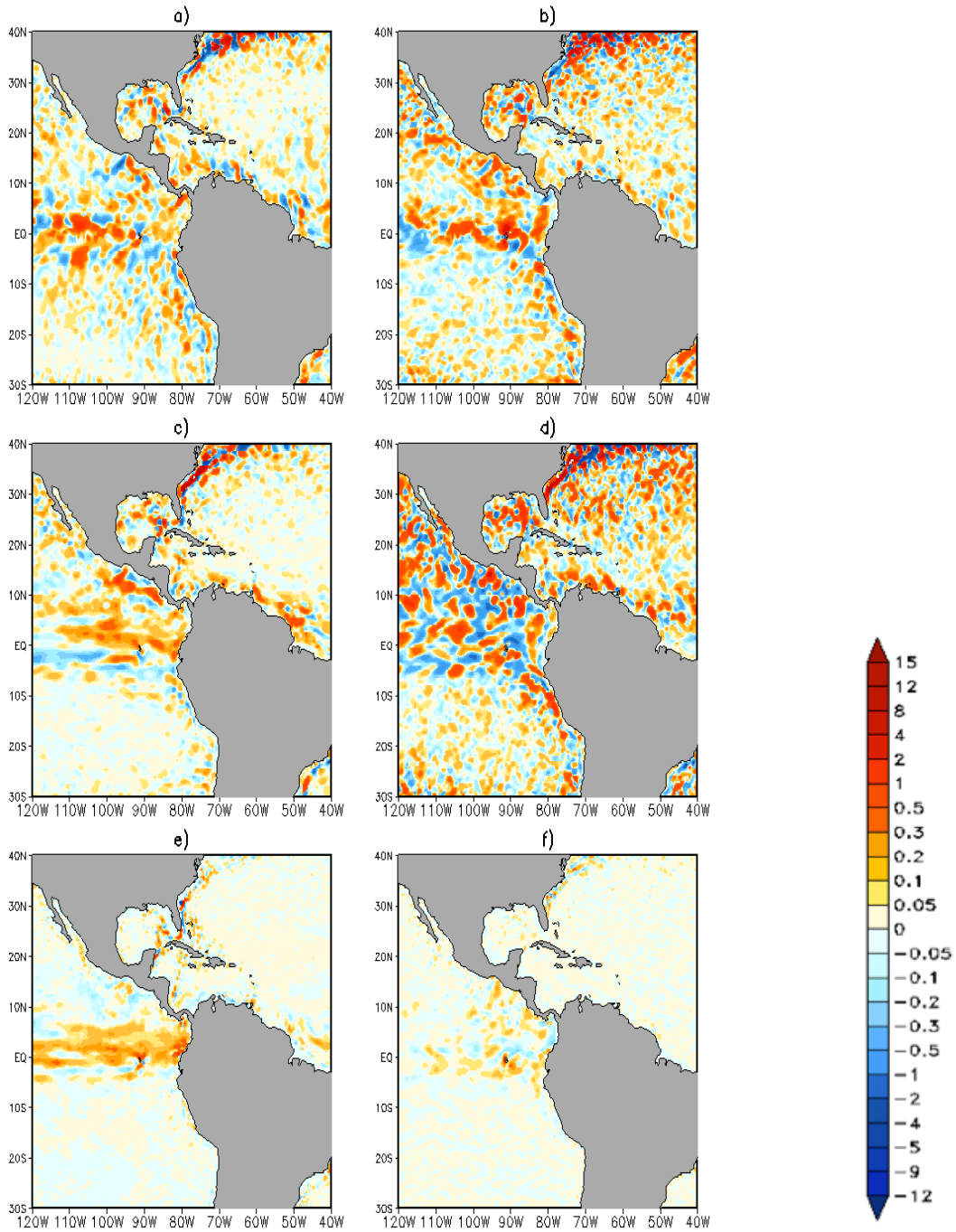


Figure 3.29. Same as Figure 3.25 but for SODA.

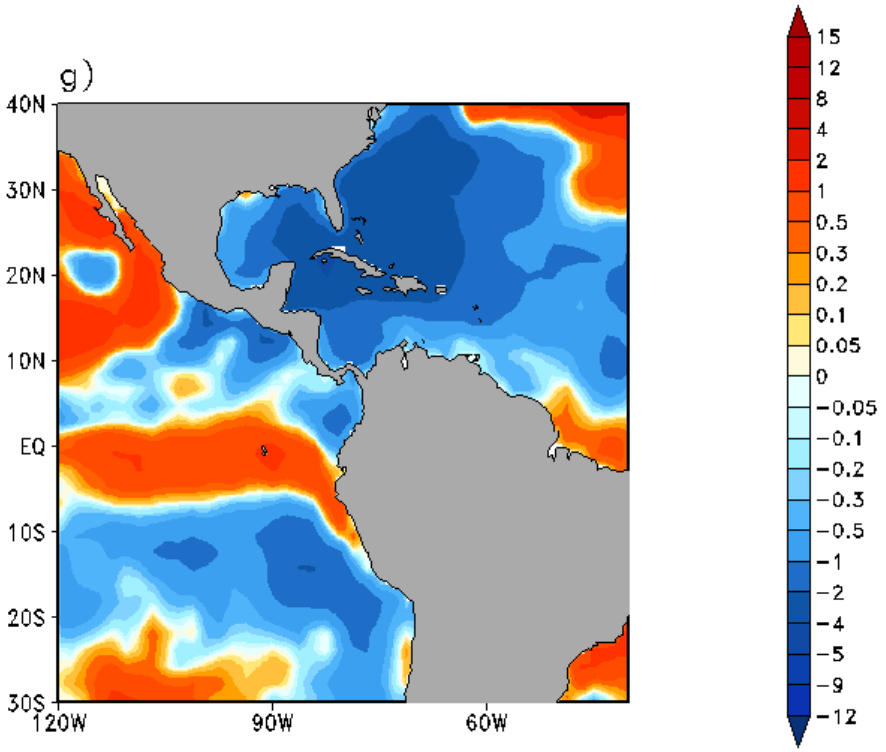


Figure 3.30. Same as Figure 3.26 but for SODA with R1.

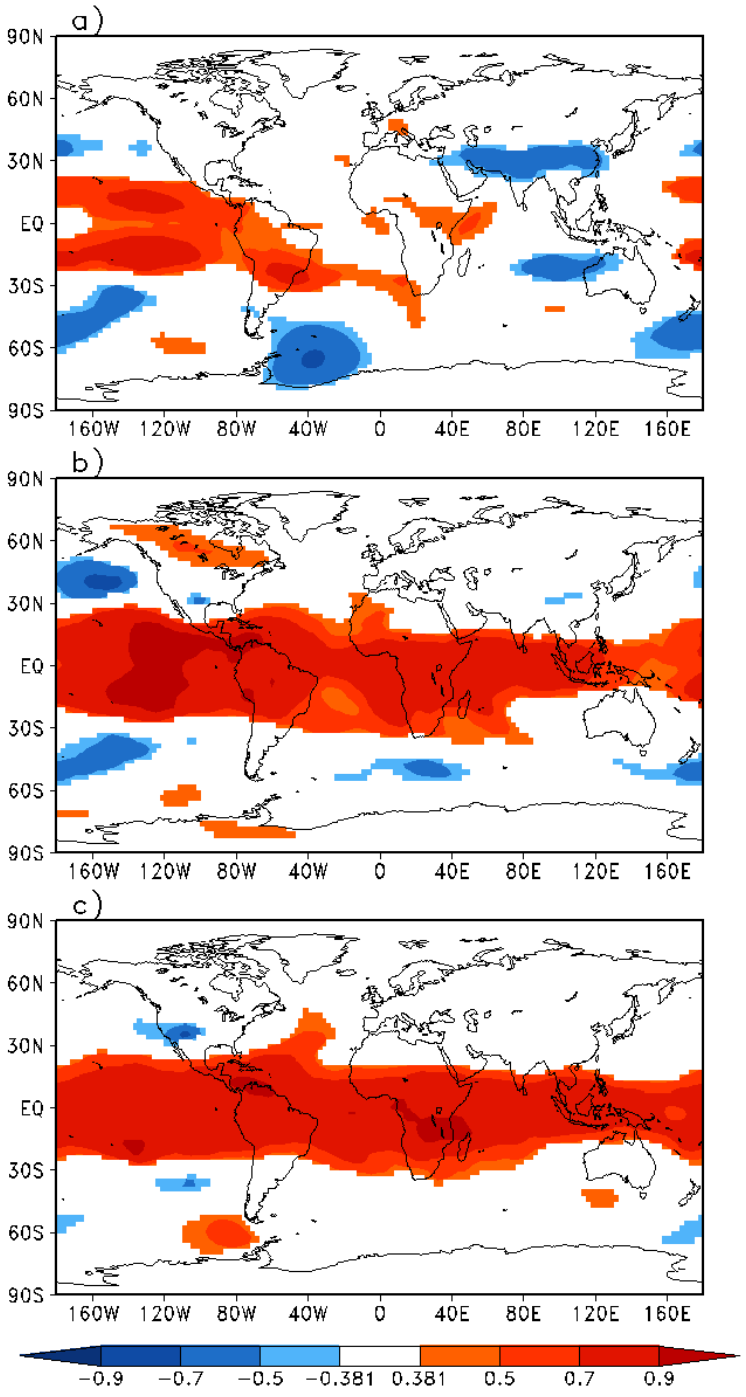


Figure 3.31. Correlation of SON Niño-3 SSTAs with the a) SON TTAs, b) DJF TTAs, and c) MAM TTAs in GODAS with R2. The Niño-3 SSTAs are leading. Only values that are greater than the 95% significance are shown. Only values that are greater than the 95% significance ( $|r| \geq 0.381$) are shown.

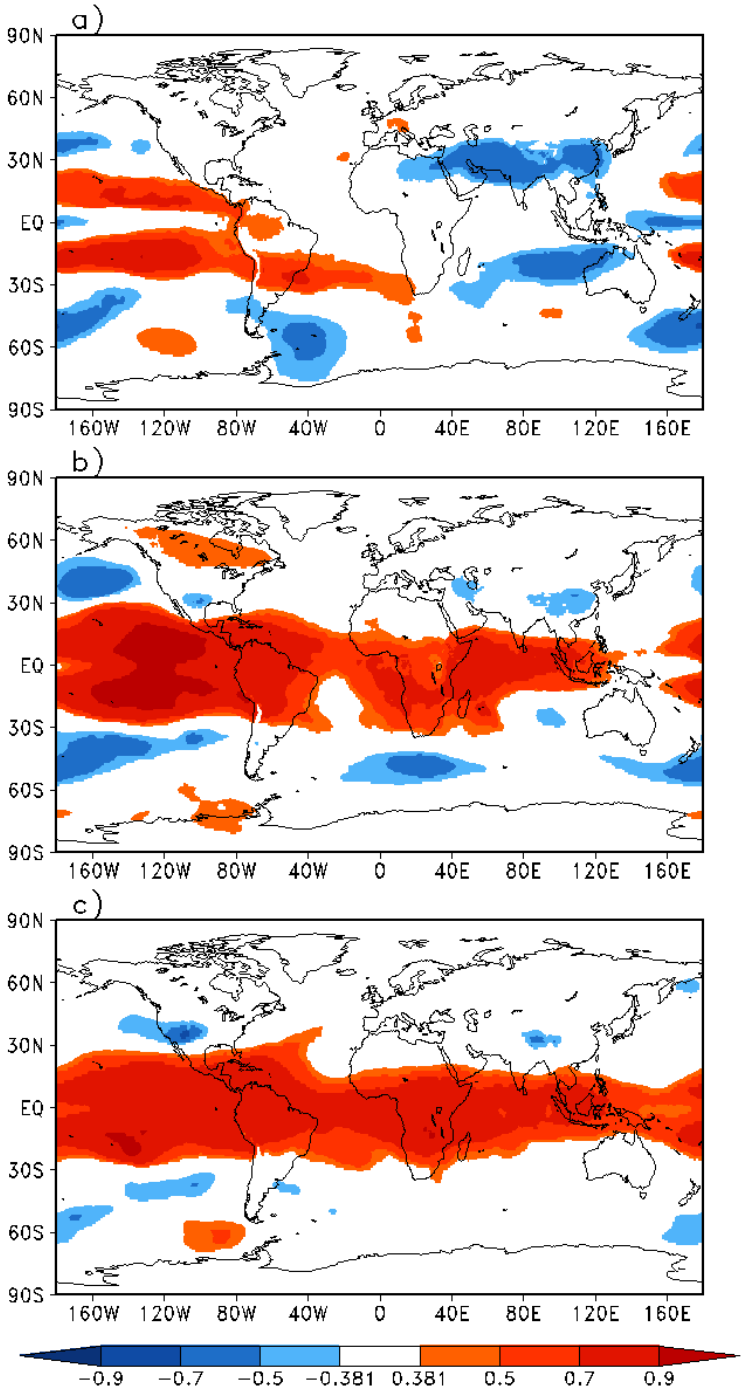


Figure 3.32. Same as Figure 3.31 but for CFSR.

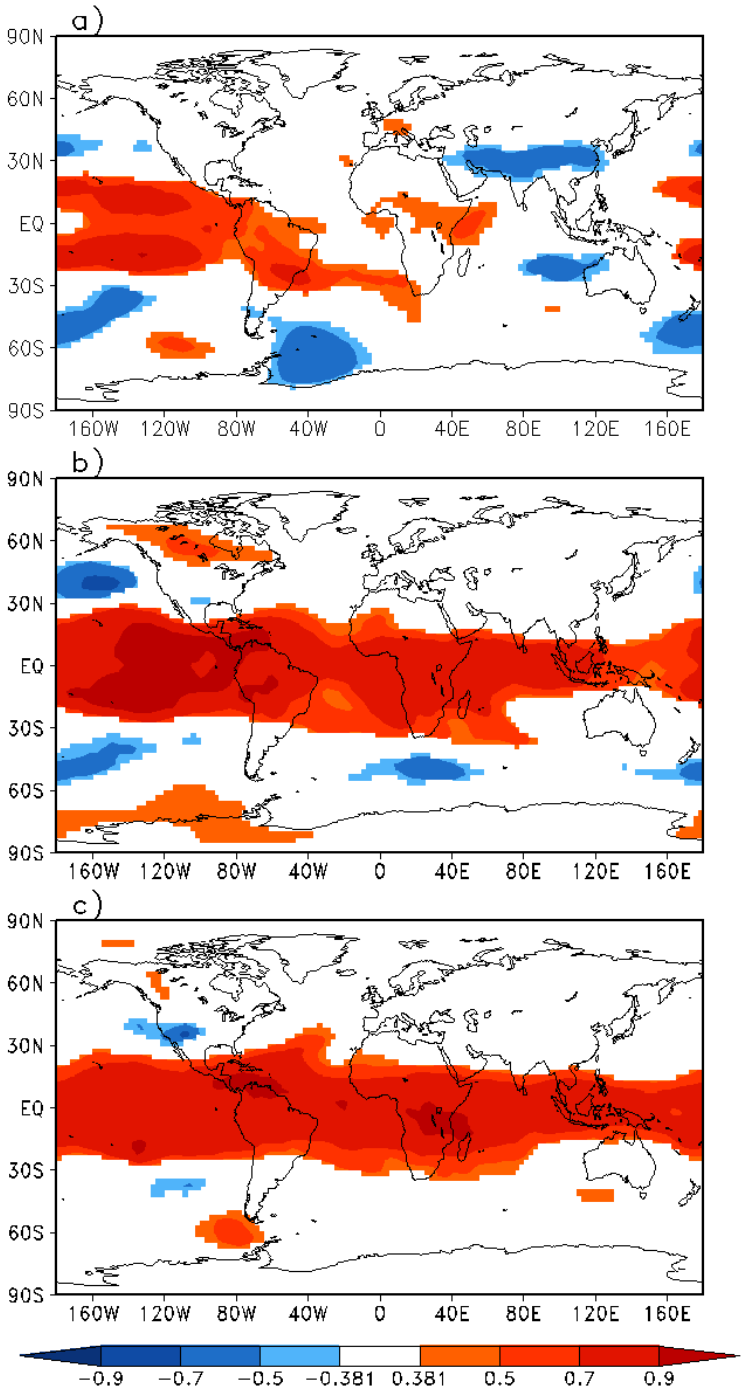


Figure 3.33. Same as Figure 3.31 but for SODA with R1.

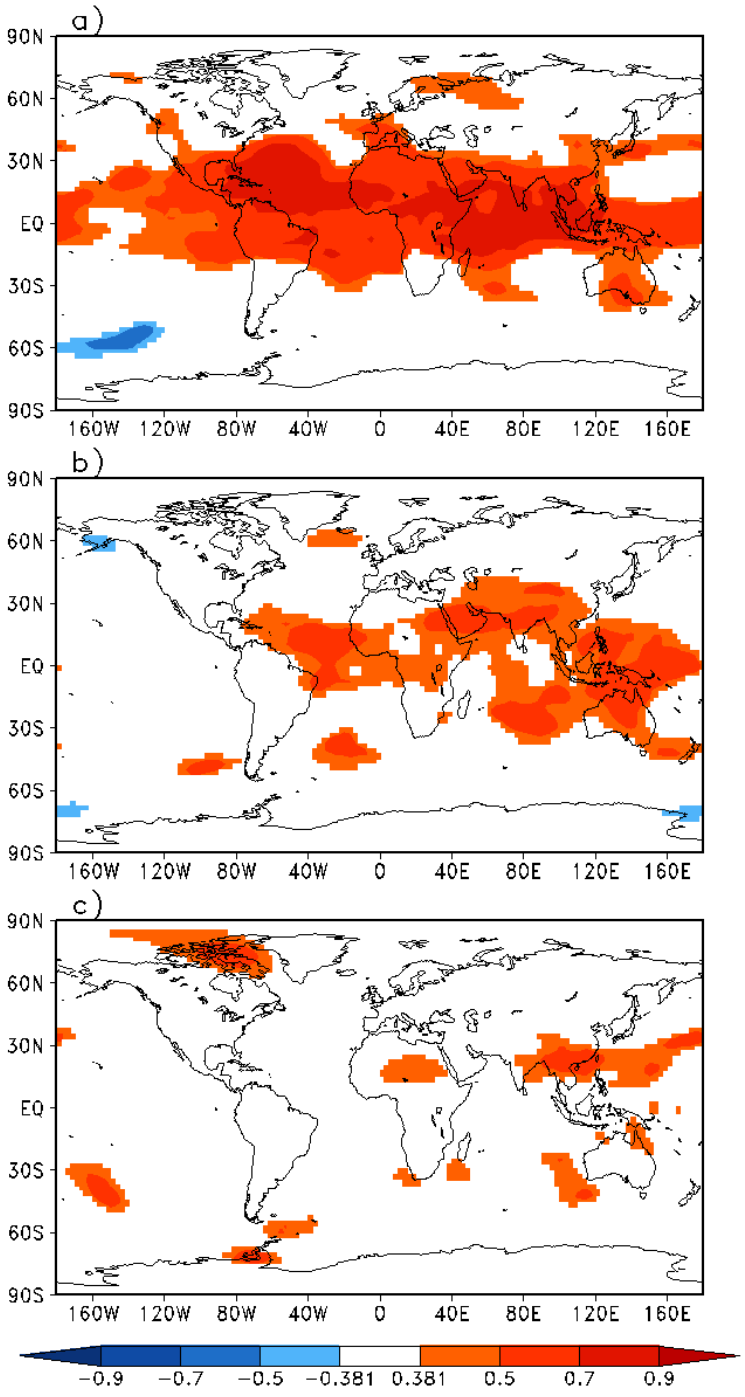


Figure 3.34. Correlation of ASO AWP area with the a) ASO TTAs, b) NDJ TTAs, and c) FMA TTAs in GODAS with R2. The AWP area is leading. Only values that are greater than the 95% significance are shown. Only values that are greater than the 95% significance ( $|r| \geq 0.381$) are shown.

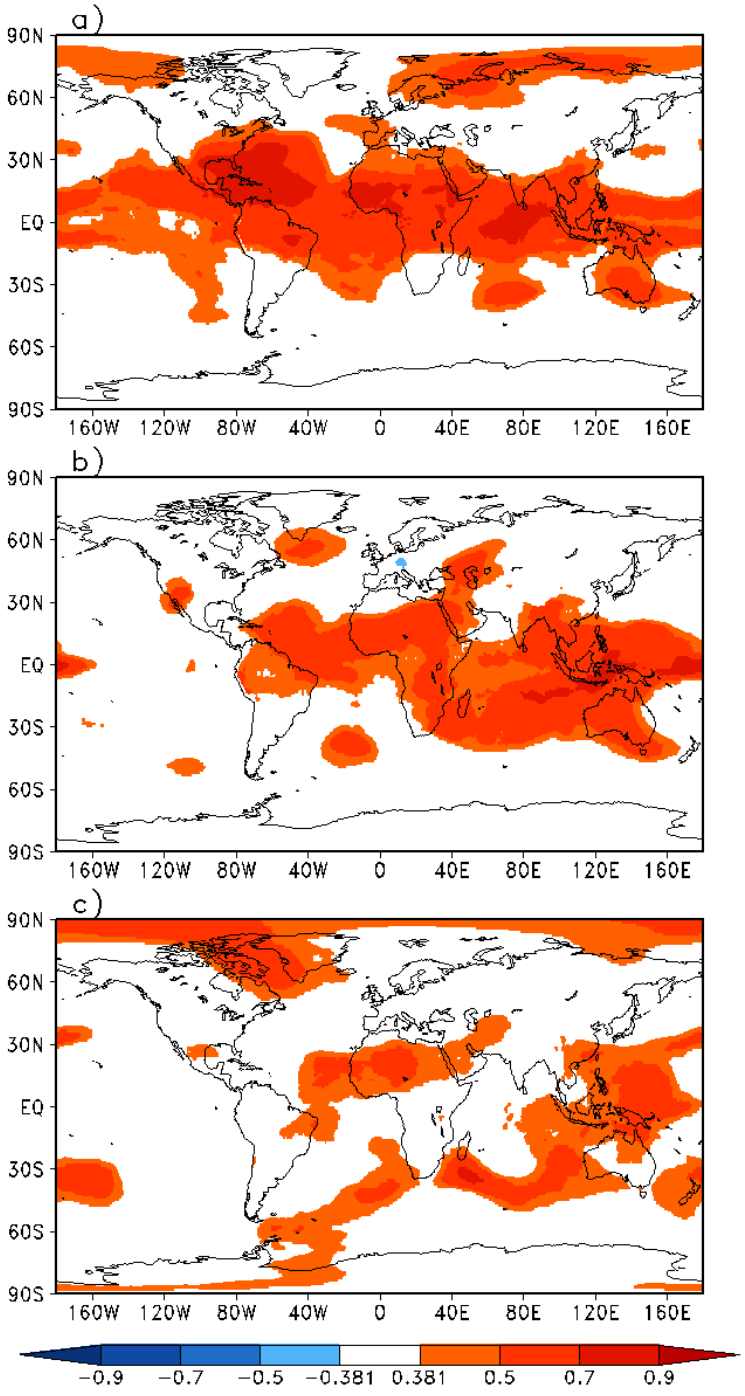


Figure 3.35. Same as Figure 3.34 but for CFSR.

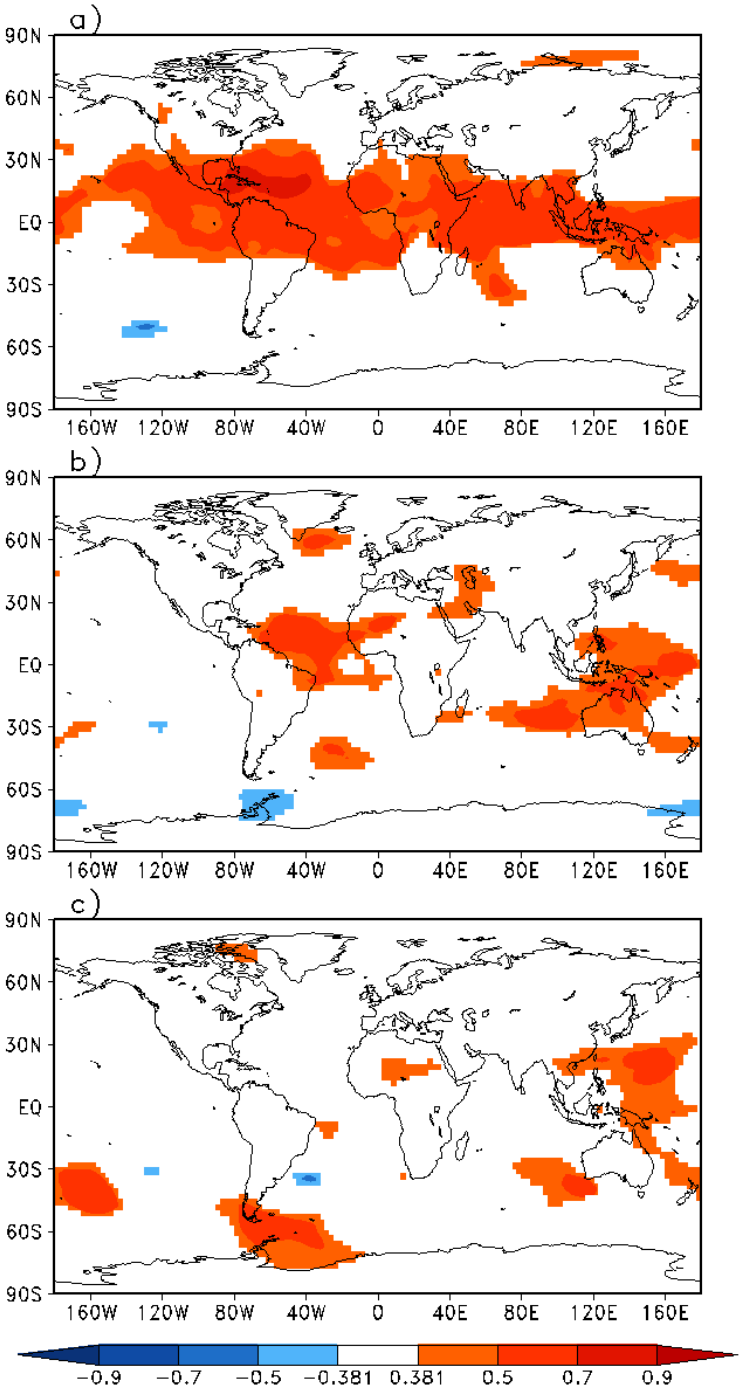


Figure 3.36. Same as Figure 3.34 but for SODA with R1.

Table 3.1 AWP area of the five years exhibiting the largest AWP area in GODAS, CFSR, and SODA. Units of the AWP area are $km^2$.

| Large AWPs | | |
|---|---|---|
| **Reanalysis** | **Year** | **Area ($km^2$)** |
| **GODAS** | 2005 | 9,151,790 |
| | 1998 | 8,889,170 |
| | 1987 | 8,481,570 |
| | 2006 | 8,101,570 |
| | 2003 | 7,769,130 |
| **CFSR** | 2005 | 9,326,050 |
| | 2006 | 7,964,990 |
| | 2003 | 7,355,780 |
| | 1998 | 7,345,160 |
| | 2004 | 6,930,590 |
| **SODA** | 2003 | 9,967,120 |
| | 2004 | 9,728,540 |
| | 1998 | 9,469,110 |
| | 1987 | 8,974,640 |
| | 1995 | 8,226,740 |

Table 3.2 AWP area of the five years exhibiting the smallest AWP area in GODAS, CFSR, and SODA. Units of the AWP area are $km^2$.

| Small AWPs | | |
|---|---|---|
| **Reanalysis** | **Year** | **Area ($km^2$)** |
| **GODAS** | 1992 | 3,294,770 |
| | 1982 | 3,191,140 |
| | 1986 | 2,950,100 |
| | 1985 | 2,511,780 |
| | 1984 | 737,938 |
| **CFSR** | 1988 | 1,711,920 |
| | 1986 | 1,709,120 |
| | 1994 | 1,674.710 |
| | 1992 | 1,616,940 |
| | 1988 | 524,063 |
| **SODA** | 1982 | 2,898,870 |
| | 1992 | 2,872,160 |
| | 1986 | 2,694,600 |
| | 1985 | 2,289,110 |
| | 1984 | 589,218 |

Table 3.3 Mean maximum depth of the 26.0°C isotherm of the five years exhibiting the largest AWP area in ASO in GODAS, CFSR, and SODA. The years for each reanalysis are from Table 3.1. Units of depth are meters.

| Large AWPs | |
|---|---|
| **Reanalysis** | **Mean Maximum Depth (meters)** |
| **GODAS** | ~148 |
| **CFSR** | ~139 |
| **SODA** | ~148 |

Table 3.4 Mean maximum depth of the 26.0°C isotherm of the five years exhibiting the smallest AWP area in ASO in GODAS, CFSR, and SODA. The years for each reanalysis are from Table 3.2. Units of depth are meters.

| Small AWPs | |
|---|---|
| **Reanalysis** | **Mean Maximum Depth (meters)** |
| **GODAS** | ~159 |
| **CFSR** | ~146 |
| **SODA** | ~156 |

# CHAPTER FOUR

# CONCLUSIONS

In this study, we examined and intercompared reanalysis' rendition of the AWP. The reanalysis products that were used were the following: (1) GODAS with R2, (2) CFSR, and (3) SODA with R1. Four analyses were examined and they were the following: (1) the annual variability of the AWP, (2) the interannual variability of the AWP, (3) an SST budget analysis of the AWP, and (4) the atmospheric response to the AWP.

We showed that the reanalyses exhibited a similar seasonal cycle of the AWP for all three reanalyses. The AWP is nonexistent in boreal winter (DJF) and at a maximum in late boreal summer (ASO). However, there were notable differences between the reanalyses: (1) the AWP appears in different months in the reanalyses; April, May, and June for the SODA, the GODAS, and the CFSR, respectively, (2) the SST fields of the SODA are less smooth in comparison to the GODAS and the CFSR, and (3) the GODAS does not have the AWP extend into the western tropical North Atlantic, whereas the CFSR and SODA do.

We showed the interannual variability of the AWP in all three reanalyses by looking at lead−lag correlations between the AWP area and SSTAs. The AWP area is positively correlated with SSTAs in the eastern subtropical North Atlantic and the western tropical North Atlantic contemporaneously, as well as at a three and six-month lead (SSTAs leading) in all three reanalyses. All three reanalyses show a positive correlation between the AWP area and SSTAs in the North Atlantic contemporaneously, as well as at a three and six-month lead and lag. Six months after (FMA), the GODAS shows no statistically significant correlations in the Gulf, Caribbean Sea, and the tropical North Atlantic. Also, the CFSR is showing positive correlations between the AWP area and the western Pacific contemporaneously, as well as three months (NDJ) and six months after (FMA). In addition, we showed the interannual variability of the AWP in all three reanalyses by looking at lead−lag correlations between the AWP area and STAs. All three reanalyses show positive correlations between the AWP area and STAs contemporaneously, and at a three and six-month lead (STAs leading), in the western tropical North Atlantic and eastern subtropical North Atlantic extending to a depth of 200 m. At a three-month lag (NDJ), all reanalyses show that STAs in the Gulf are not positively correlated with the

AWP area. All three reanalyses showed a relationship between the AWP area and the STAs south of Greenland, however, the depth at which STAs were significantly correlated were different for all reanalyses.

We showed that in all three reanalyses, the mean maximum depth of the 26.0°C isotherm is larger in small AWPS than large AWPs in ASO. In addition, the 26.0°C isotherm is deeper in the Caribbean Sea, the western tropical North Atlantic, and the Gulf for small AWPs than large AWPs in ASO. Thus, in ASO, small AWPs have a higher hurricane heat potential than large AWPs. GODAS and SODA showed similar results compared to CFSR.

It was shown that in GODAS and CFSR, the flux terms contribute more to the AWP SST tendency, whereas the advective terms in the SODA are the main contributor to the AWP SST tendency. All reanalyses show advective terms in the eastern Pacific, as well as advective terms collocated with the Gulf Stream and the Loop Current, contributing to the AWP SST tendency

Lastly, we showed that in all three reanalyses, the AWP does not warm the tropical troposphere three to six months after the AWP (ASO) in the same way that an ENSO event does. However, the tropical troposphere is warmed contemporaneously (ASO) with correlation values between 0.5 and 0.7 in the tropical Atlantic in the Gulf, Caribbean Sea, and tropical North Atlantic. Three months after, the correlation values in the tropical Atlantic are lower with values between 0.381 and 0.5. Six months after, the CFSR is the only reanalysis with positive correlations in the eastern tropical Atlantic with values between 0.381 and 0.5.

There are numerous opportunities of future work stemming from this study. First, one can look at more reanalysis products and see if they are producing similar renditions of the AWP. Second, other methods can be used to examine the AWP SST tendency. Additionally, it would be helpful to look at the contribution of the fluxes to the AWP SST tendency individually, i.e., longwave radiation, shortwave radiation, latent heat flux, and sensible heat flux. Lastly, on scales beyond purview of this study, more research is necessary to accurately describe the correlations that were seen between the AWP area and SSTAs, STAs, and TT anomalies. We were able to determine if there is a relationship between the AWP area and SSTAs, STAs, and TT anomalies in all reanalyses, however, correlations do not imply causation. Thus, additional works needs to be done to describe the correlations. Some examples are the following: (1) the relationship between the AWP area and North Atlantic SSTs could be a sign of the Atlantic Multidecadal Oscillation, (2) the relationship between the AWP area and the Pacific SSTs (in CFSR) could be

a sign of a the Pacific Decadal Oscillation or a sign of a Pacific/North American related dependency, (3) the relationship between the AWP area and the North Atlantic water to depths of ~4000 m (in CFSR) could be a sign of deep water formation, (4) the relationship between the AWP area and the STAs off the coast of South America could be from outflow from the Orinoco and Amazon rivers, and (5) the relationship between the AWP area and the STAs extending to a depth of 200 m in the western tropical North Atlantic and the eastern subtropical North Atlantic could be a sign of Mediterranean outflow. However, these are merely suggestive relationships and should be further examined.

# REFERENCES


Behringer, D.W., and Y.Xue, 2004: Evaluation of the global ocean data assimilation system at NCEP: The Pacific Ocean. 8th symposium on integrated and observation system for the atmosphere, ocean and land surface, AMS 84th annual meeting, Washington Sate Convention15 and Trade Center, Seattle, Washington 11-115.

Bender, M.A., and I. Ginnis, 2000: Real-case simulations of hurricane-ocean interaction using a high resolution coupled model: Effects on hurricane intensity. *Mon. Wea. Rev.*, **128**, 917-946.

Carton, J.A., and B.S. Giese, 2008: A reanalysis of ocean climate using simple ocean data assimilation (SODA). *Mon. Wea. Rev.,* **136**, 2999-3017.

_____, G. Chepurin, and X. Cao, 2000a: A simple ocean data assimilation analysis of the global upper ocean 1950-95. Part 1: Methodology. *J. Phys. Ocean.*, **30**, 294-309.

_____, _____, and _____, 2000b: A simple ocean data assimilation analysis of the global upper ocean 1950-1995. PartII: Results. *J. Phys. Ocean.,* **30**, 311-326.

Chiang, J.C.H, and A. H. Sobel, 2002: Tropical tropospheric temperature variations caused by enso and their influence on the remote tropical climate. *J. Climate*, **15**, 2616-2631.

Davis, Robert. E., B. P. Hayden, D. A. Gray, W. L. Phillips, and G. V. Jones, 1997: The North Atlantic Subtropical Anticyclone. *J. Climate*, **10**, 728-744.

Derber, J.C., and A. Rosati, 1989: A global oceanic data assimilation system. *J. Phys. Oceanogr.*, **19**, 1333-1347.

Gill, A.E., 1980: Some simple solutions for heat-induced tropical circulation. *Quart. J. Meteor. Soc.*, **106**, 447-462.

Gray, W.M., 1979: Hurricanes: Their formation, structure, and likely role in the tropical circulation. *Meteorology over the Tropical Oceans*, D. B. Shaw, Ed., Royal Meteorlogical Society, 155-218.

Holland, Greg. J: The maximum potential intensity of tropical cyclones. *J. Atmos. Sciences*, **54**, 2519-2541.

Kanamitsu, M., and Coauthors, 2002: NCEP-DOE AMIP-II Reanalysis (R-2). *Bull. Amer. Meteor. Soc.*, **83**, 1631-1643.

Kalnay, E., et al., 1996: The NCEP/NCAR 40-year reanalysis project. *Bull. Americ. Meteor. Soc.*, **77**, 437-471.

Kang, I.-S., I.-S. An, and F.-F. Jin, 2001: A systematic approximation of the sst anomaly

equation for enso. *J. Meteor. Soc.*, **79**, 1–10.

Kleist, D. T., D. F. Parrish, J. C. Derber, R. Treadon, R.M Errico, and R. Yang, 2009: Improving incremental balance in the gsi 3dvar analysis system, *Mon. Wea. Rev.*, **137**, 1046-1060.

Knaff, J.A., 1997: Implications of summertime sea level pressure anomalies in the tropical Atlantic region. *J. Climate,* **10**, 789-804.

Leipper, D., and D. Volgenau, 1972: Hurricane heat potential of the Gulf of Mexico. *J. Phys. Oceanogr.*, **2**, 218–224.

Lewsey, C., G. Cid, and E. Kruse, 2004: Assessing climate change impacts on coastal infrastructure in the eastern caribbean. *Marine Policy*, **28**, 393-409.

Misra, V., L. Marx, M. Fennessy, B. Kirtnman, and J. L. K. III, 2008: A comparison of climate prediction and simulation over the tropical pacific. *J. Climate*, **21**, 3601–3610.

Pacanowski, R.C and S.M. Griffies, 1998: MOM 3.0 Manual. NOAA/Geophysical fluid dynamics laboratory. Princeton, NJ. USA 08542.

Parrish, D.F and J.C. Derber, 1992: The national meteorological center's spectral statistical interpolation analysis system. *Mon. Wea. Rev.*, **120**, 1747-1763.

Reynolds, R. W., N.A Rayner, T.M. Smith, D.C. Stokes, W.Wang, 2002: An improved in situ and climate satellite SST analysis for climate. *J. Climate*, **15**, 1609-1625.

Reynolds, R.W., T.M. Smith, C. Liu, D. B. Chelton, K. S Casey, and M. G Schlax, 2007: Daily high-resolution blended analyses for sea surface temperature. *J. Climate*, **20**, 5473-5496.

Saha, S., et al., 2010: The NCEP Climate Forecast System Reanalysis. *Bull. Ameri. Meteor. Soc.*, **91**, 1015-1057.

Shay, L.K., G.J. Goni, and P.G. Black, 2000: Effects of a warm oceanic feature on Hurricane Opal. *Mon.Wea. Rev.*, **128**, 1366-1383.

Smith, R.D., J.K. Dukowicz, and R.C. Malone, 1992: Parallel ocean general circulation modeling. *Physica D.*, **60**, 38-61.

Vimont, D. J., and J. P. Kossin, 2007: The atlantic meridional mode and hurricane activity. *Geophys. Res. Lett.*, **34**, doi:10.1029/2007GL029683.

Wang, C., and D. B. Enfield, 2001: The tropical western hemisphere warm pool. *Geophys. Res. Lett.*, **28**, 1635 – 1638.

_____, and _____, 2003: A further study of the tropical western hemisphere warm pool, *J. Clim.*, **16**, 1476 – 1493.

Wang, C., D.B. Enfield, S-K. Lee, and C.W. Landsea, 2006: Influence of the atlantic warm pool on western hemisphere summer rainfall and atlantic hurricanes. *J. Climate*, **19**, 3011-3028.

Wang, C. and S-K. Lee, 2007: Atlantic warm pool, caribbean low-level jet, and their potential impact on hurricanes. *Geophys. Res. Lett.*, **34**, doi: 10.1029/2006GL028579.

Wang, C., S-K. Lee, and D.B. Enfield, 2008: Climate response to anomalously large and small atlantic warm pools during the summer. *J. Climate*, **21**, 2437-2450.

_____, _____, and _____, 2007: Impact of the atlantic warm pool on the summer climate of the western hemisphere. *J. Climate*, **20**, 5021-5040.

Wu, X., K.S Morthi, K. Okomoto, and H. L. Pan, 2005: Sea ice impacts on gfs forecasts at high latitudes. Proceedings of the 85th AMS Annual Meeting, 8th Conference on Polar Meteorology and Oceanography, San Diego, Ca.

Zheng, Y. and B.S. Giese, 2009: Ocean heat structure in simple ocean data assimilation: structure and mechanism. *J. Geophys. Res.*, **114**, doi: 10.1029/2008JC005190.

# BIOGRAPHICAL SKETCH

Ashley Stroman was born in Abbington, Pennsylvania on August 26, 1985. She then lived in New Orleans, La until the age of 11 before moving to Jacksonville, Fl. Living in Louisiana and Florida greatly influenced her interest in Meteorology. She graduated from Orange Park High School in 2003, and then graduated from the University of Central Florida in 2008 with a Bachelors Degree in Applied Mathematics. She then decided to pursue her interest in Meteorology and opted to attend graduate school at The Florida State University. She began working with Dr. Misra in her second year and her research includes the Atlantic Warm Pool. After graduating with her Masters Degree, she plans to go for her Ph.D in Oceanography at The Florida State University. In her free time, she enjoys being outside, reading, and spending time with family and friends.